Available online at www.sciencedirect.com
SCIENCE DIRECT
ELSEVIER
Icarus 183 (2006) 451–470
ICARUS
www.elsevier.com/locate/icarus

Deuterium chemistry and airglow in the jovian thermosphere

C.D. Parkinson [a,c,*], J.C. McConnell [b], L. Ben Jaffel [c], A.Y.-T. Lee [a], Y.L. Yung [a], E. Griffioen [b]

[a] *Division of Geological and Planetary Sciences, California Institute of Technology, 1200 E. California Blvd., Pasadena, CA 91125, USA*
[b] *Department of Earth and Atmospheric Science, York University, North York, Ontario, M3J 1P3, Canada*
[c] *Institut d'Astrophysique de Paris–CNRS, 98bis Blvd. Arago, 75014 Paris, France*

Received 23 February 2004; revised 20 September 2005

Available online 21 June 2006

Abstract

We present a detailed study of the distribution of key deuterated species (viz., atomic D and HD) and the associated deuterium Lyman-α airglow in the jovian thermosphere. The reactions that appear to govern the abundances of these deuterated species are used in conjunction with C_2-chemistry in a 1-D photochemical-diffusion model. While the D abundance is mainly sensitive to H densities and the vibrational temperature profile, the D vertical distribution also depends on other parameters such as eddy mixing and the uncertain values of some of the reaction rate constants. We consider different scenarios by varying several parameters controlling the D distribution in the thermosphere. A radiative transfer model with coupling of the H and D Lyman-α lines is employed to obtain line profiles and total intensities at disk center for these scenarios. This allows a comparison of the impact of various parameters on the jovian D Lyman-α emission. A consequence of these chemical processes in the jovian thermosphere is the formation of CH_2D, CH_3D, and C_2H_5D, and other deuterated species. We also discuss the source of these deuterated hydrocarbons and their abundance. We find that HD vibrational chemistry impacts D in the thermosphere, CH_3D and C_2H_5D are vibrationally enhanced in the thermosphere, and variations in abundance of CH_3D and C_2H_5D in the thermosphere may reflect dynamical activity (i.e., K_h) in the jovian upper atmosphere. An observing program dedicated to providing such measurements of these testable phenomena would provide further insight into the synergistic coupling between chemistry, energetics and airglow in the jovian upper atmosphere.

Keywords: Jupiter, atmosphere; Photochemistry; Radiative transfer; Abundances, atmospheres

1. Introduction

The D/H abundance has important implications for the evolution of the Solar System and until recently the only inferences of the ratio on the giant planets has been by CH_3D spectroscopy (e.g., Beer and Taylor, 1973, 1978) and measuring the pressure induced HD line (Trauger et al., 1973). Recently in situ measurements of the (D/H) ratio on Jupiter have been made by the Galileo Probe Mass Spectrometer (GPMS) (Mahaffy et al., 1998), as well as HD spectroscopic measurements from the Long Wavelength Spectrometer (LWS) on the Infrared Space Observatory (ISO) (Lellouch et al., 1996). The work described in this paper was motivated by a tentative observation of the D Lyman-α emission on the dawn limb of Jupiter (Ben Jaffel et al., 1998). It is an extension of the work of Parkinson et al. (1999) and addresses the uncertainties involved in of the abundance and airglow intensities of D in the jovian thermosphere.

HD from the lower atmosphere is mixed upward into the thermosphere where it can be dissociated by atomic hydrogen. Some of the resultant D atoms are subsequently lost by reactions with H_2 and CH_3 which in turn are partially converted to CH_2D, CH_3D, C_2H_5D and other deuterated hydrocarbon species (cf. Parkinson et al., 1999; Lee and Yung, 2001). Cravens (1987) and Majeed et al. (1991) have shown that vibrationally excited H_2 is important in the jovian thermosphere. Lower densities in the jovian thermosphere imply slow quenching of excited H_2, H_2^*, resulting in reduced sinks for vibrationally hot H_2. Hence, we assume that VV energy transfer from the first vibrational level of molecular hydrogen, H_2^1, which results in the excitation of vibrationally excited HD, is also present in the jovian thermosphere. The energy source is currently unknown and so it remains a challenge to identify where

* Corresponding author.
E-mail address: cdp@gps.caltech.edu (C.D. Parkinson).

0019-1035/$ – see front matter
doi:10.1016/j.icarus.2005.09.022

it comes from (Shemansky et al., 2003). As shown in detail later, the D distribution in the thermosphere is most sensitive to the H profile and the vibrational excitation of HD. While calculating the D distribution, the modeling process must produce an H atom distribution that corresponds to the best current estimates in the literature and this is done by assuming that the dayside H Lyman-α emergent intensities (airglow) can be used to adequately characterize the H distribution. Ben Jaffel et al. (1993) have used line shape measurements to constrain H distributions and excitation mechanisms and we have adopted their approach which yields a total H column of 3.7×10^{17} cm^{-2} and a non-thermal H component of $\sim 2 \times 10^{15}$ cm^{-2} above the thermopause. This value is in no way a canonical value for Jupiter, but is representative of the H column at about 10° latitude in the vicinity of the H-bulge.

The D distribution is also dependent on the distribution of CH_3. The main production of CH_3 radicals is from the photodissociation of methane. CH_3 loss is mostly via self-recombination to form ethane (C_2H_6) and with H to reform CH_4. The methyl abundance is strongly dependent upon the degree of eddy mixing, which determines the location of the methane homopause where most of the CH_3 is produced and lost. However, the self-recombination reaction rate of CH_3 at low jovian temperatures (Bézard et al., 1999; Atreya et al., 1999) is uncertain. We use the rate given by Romani et al. (1993) in this study.

Formation of CH_3D via the intermediate species CH_2D and H, is a sink for D. Some of the CH_3D goes back to CH_2D and the details of the investigation of the CH_3D distribution in the thermosphere are given below; we assume that the CH_3D mixing ratio at the bottom of the thermosphere to be 2.5×10^{-7} (Encrenaz et al., 1996).

We proceed by investigating the impact of uncertainties in eddy diffusion, HD mixing ratio, temperature profile (for T and T_v) and various critical reaction rate constants on the D abundance and on the expected D emission on the disk of Jupiter. In the following section we describe these parameters and their relation to the photochemical and radiative transfer modeling. This is followed by a presentation of the modeling results in the context of these parameters and a discussion of the implications of the calculations.

2. Description of models

For the reasons given above it is necessary to model both H and D density distributions simultaneously. Thus we use a chemical model to produce an atmosphere with number densities of key species as a function of temperature and altitude. Then we use this atmosphere in conjunction with radiative transfer models (Griffioen et al., 1994; Griffioen, 2000) to quantify estimates of the deuterium Ly-α airglow in the thermosphere of Jupiter. These models are described in more detail below.

Our standard reference model atmosphere parameters are: He mixing ratio, $f_{He} = 0.136$ (von Zahn and Hunten, 1996); HD mixing ratio, $f_{HD} = 4.5 \times 10^{-5}$ (Mahaffy et al., 1998); CH_3D mixing ratio, $f_{CH_3D} \sim 2.5 \times 10^{-7}$ (Encrenaz et al., 1996); CH_4 mixing ratio, $f_{CH_4} = 1.8 \times 10^{-4}$ (Niemann et al., 1996); eddy diffusion at the homopause, $K_h = 2 \times 10^6$ cm^2 s^{-1} (Vervack et al., 1995); H column density $\sim 3.7 \times 10^{17}$ cm^{-2} (Ben Jaffel et al., 1993), H Lyman-α solar flux of 4.4×10^6 cm^{-2} s^{-1} at 1 AU corresponding to solar maximum conditions (Tobiska, 1991, 1994); and exospheric temperature, $T_{ex} = 1100$ K based on the Voyager solar occultation results (Broadfoot et al., 1989). Cravens (1987) and Majeed et al. (1991) estimate H_2 effective vibrational temperatures between 1300 and 4000 K depending on altitude and vibrational level; we have taken $T_v = 3T$ as a standard reference which approximately corresponds to this range of values. We note that Waite et al. (1983) have calculated T_v for auroral regions to be $\sim$3000 K in the topside ionosphere.

The standard reference atmosphere used for this paper uses the CH_4 and HD mixing ratios from the GPMS experiment which are different from those used by Parkinson et al. (1999). This results in a reduced D concentration overall and lower D Lyman-α emergent intensities for the various cases given the same conditions in that paper.

2.1. Temperature

There are few direct measurements of the temperature profile in the jovian upper atmosphere, and our knowledge of heating processes is insufficient to provide information in the geographical and diurnal variation of thermospheric temperatures. For our calculations we have adopted a standard reference temperature profile based on the deceleration data obtained by the Galileo Probe (Seiff et al., 1997), which goes from 24 bar to $\sim$0.01 mbar. We nominally choose an exospheric temperature of 1100 K, which is compatible with the Voyager UVS measurements (Broadfoot et al., 1981, 1989) and Galileo Probe measurements (Seiff et al., 1997). For comparison we also consider the temperature profile used by Romani (1996) in some of our calculations. His temperature profile is based upon: Voyager IRIS observations of Jupiter's southern midlatitudes for the pressure range 500 to 0.1 mbar; isothermal (173 K) between 0.1 mbar and 1 μbar; and for pressures less than 1 μbar a thermal gradient of 1 K km^{-1} (Festou et al., 1981). The same UVS occultation data was reanalyzed by Yelle et al. (1996) using a thermal gradient of 3 K km^{-1}, consistent with the range of temperatures derived by Seiff et al. (1997) using the Galileo Probe data. However, we use the Romani (1996) profile for comparative purposes since we are interested in considering an atmospheric temperature profile that is cooler than that obtained by the Galileo Probe measurement (Seiff et al., 1997), and in no way regard the Romani (1996) temperature profile as canonical. Both temperature profiles are displayed in Fig. 1a. Since the temperature profiles are quite different we have done some of the calculations for D chemical profiles using both T profiles. This provides a diagnostic to test the sensitivity of the results to the temperature profile chosen, since both kinetic and vibrational temperature profiles will be affected (cf. Figs. 1a and 1b).

Ideally, T_v for H_2 and HD should be calculated simultaneously with the D chemistry. We hope to do this eventually, but as we show below, the HD vibrational temperature is tightly coupled to the H_2 vibrational temperature, and so, to allow for

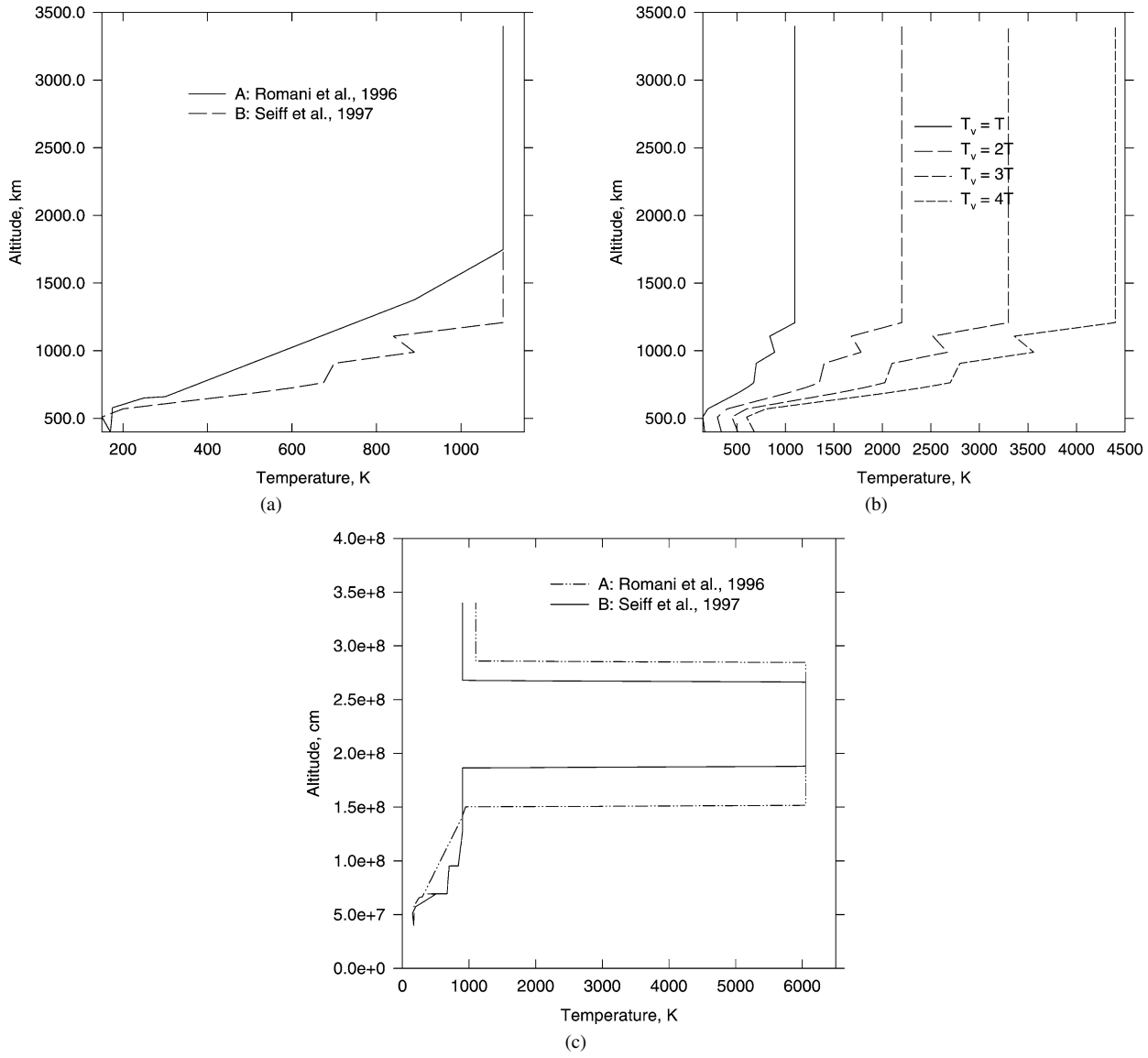

Fig. 1. Temperature profiles adopted for the mesosphere and thermosphere of Jupiter. (a) The Romani (1996) temperature curve is based upon Voyager IRIS observations of Jupiter's southern midlatitudes (profile A). The other temperature profile is taken from Seiff et al. (1997) (profile B). See text for details. (b) Various vibrational temperature profiles corresponding to $T_v = nT$, where $n = 1$ to 4. See text for details. (c) Same as (a) except bulge region shown included.

a 'reasonable' variation of T_v, we adopt T_v between 1 and 4 times kinetic. The role of this in the deuterium chemistry is discussed in detail below. Fig. 1b shows the various vibrational temperature profiles that were considered for this study, viz., $T_v = nT$ as previously defined. The H_2 effective vibrational temperatures of Cravens (1987) and Majeed et al. (1991) are used as a guide.

We initially represented the H Lyman-α airglow by two regions, a non-bulge region where the solar maximum subsolar intensity is ~12 kR and a bulge region where the subsolar intensity is ~18 kR for solar maximum conditions (Sandel et al., 1980; Clarke et al., 1991; McGrath, 1991; Ben Jaffel et al., 1993). We assumed that in the non-bulge region intensities are due to an H column of $\sim 3.7 \times 10^{17}$ molecules cm^{-2} excited by the solar Lyman-α line. Following Ben Jaffel et al. (1993) we assumed that for the bulge region the excess intensity is due to a column of $\sim 2 \times 10^{15}$ molecules cm^{-2} of 'hot' hydrogen which may be represented by an effective temperature ~6050 K. For our calculations in this region we assumed the existence of a layer of the atmosphere where the temperature increases from the background to 6050 K and extends vertically over an H column of $\sim 2 \times 10^{15}$ cm^{-2} (cf. Fig. 1c). This temperature corresponds to a turbulent velocity, $V_t \sim 10$ km s^{-1}. The relationship between V_t and temperature is taken from

$$V_t^2 = \frac{2kT_{tot}}{m}, \tag{1}$$

where $T_{tot} = T_{hot} + T_{neutral}$, $T_{neutral}$ is the background temperature, T_{hot} is temperature corresponding to the hot H column, k is Boltzmann's constant and m is the mass of H. This is clearly an oversimplification of the physical situation, but it should yield reasonable results for our numerical experiments. An investigation into the effect of the location of the 'hot' region versus altitude was carried out and will be discussed in a later section.

2.2. Eddy diffusion

The standard value for the eddy diffusion coefficient at the homopause, K_h, adopted herein is based on a reanalysis of the Voyager He 584 Å airglow data (Vervack et al., 1995) which yielded a value of $K_h \sim 2^{+2}_{-1} \times 10^6$ cm^2 s^{-1}. As the eddy diffusion profile, K_z, varies with height, z, we consider a profile such that $K_z = K_h$ above the homopause (at height z_h) and $K_z = K_h\sqrt{n_{bg}(z_h)/n_{bg}(z)}$ below z_h where $n_{bg}(z)$ is the background density at height level z (cf. Parkinson et al., 1998). Molecular diffusion coefficients are taken from Mason and Marrero (1970) and Atreya (1986) where applicable. A range of values for K_h is explored.

2.3. Solar flux and line shape

The solar Lyman-α line shape is important for the excitation of D Lyman-α. H Lyman-α has been measured by Lemaire et al. (1978) and we use the empirical approximation to the line shape function suggested by Gladstone (1988). The solar line flux is given by

$$S(x) = \frac{\pi F}{2\sqrt{\pi}x_{dis}}\left(e^{-((x-x_{off}-x_r)/x_{dis})^2} + e^{-((x+x_{off}-x_r)/x_{dis})^2}\right), \tag{2}$$

where πF is the total flux in the line incident on the upper boundary of the atmosphere. x is the wavelength value from line center, x_{off} is the offset of the Gaussian curves from line center, x_{dis} is a measure of the width of the line (dispersion), all measured in Doppler units, and

$$x_r = \Delta + \frac{\lambda R\Omega \cos\theta \sin\Phi}{c} \tag{3}$$

accounts for the Doppler shift due to planetary rotation. λ is the line center frequency of interest, Δ is the frequency difference between H Lyman-α and D Lyman-α, θ is the planetary solar latitude, and Φ is the planetary solar longitude. We have ignored the 3° inclination of Jupiter's rotation axis. Values for πF, x_{off}, x_{dis}, the width in angstroms of an standard Doppler unit at a reference temperature of 500 K, and Δ are listed in Table 1. These have been adjusted from Gladstone (1988) to provide an adequate fit to the solar intensity in the vicinity of the D Lyman-α line (cf. Vidal-Madjar, 1975). For four years starting in 1969, solar Lyman-α flux measurements were made by an experiment on the OSO-5 spacecraft (Vidal-Madjar, 1975). This experiment yielded information on the total Lyman-α flux, the central Lyman-α flux, the blue wing flux at D Lyman-α, and the slope of D Lyman-α at the same location, which helps us to overcome one previously unresolvable aspect of solar UV irradiance variation: the line shape of the H Lyman-α solar line and its variability with solar activity. Solar ultraviolet irradiance variations have been discussed by Lean (1987, 1991) who notes that the mechanisms for the variability are not completely understood nor adequately determined experimentally. For instance, a variation of ~36% was observed during one month in July during 1982. Lean (1987) illustrates that there are differences in the widths of two profiles shown in Meier and Prinz (1970) and Lemaire et al. (1978) for a 'quiet' Sun. These differences need to be resolved owing to the importance of the profile for calculations of Lyman-α absorption in a wide variety of phenomena in our Solar System. An additional confounding factor is that the Atmospheric Explorer E (AE-E) and Solar Mesosphere Explorer (SME) data sets do not overlap and appear to disagree (Lean, 1987, 1991). This increases the difficulty of obtaining a value for the solar flux as determined by various solar EUV irradiance models (Tobiska, 1991, 1994; Richards et al., 1994) as discussed by Bush and Chakrabarti (1995) and Parkinson et al. (1998). Certainly, the total solar flux appears to have an upper bound of ~5×10^{11} photons cm^{-2} s^{-1} for solar maximum conditions at 1 AU. We adopt the value of 4.4×10^{11} photons cm^{-2} s^{-1} for the solar maximum as a standard for our calculations. We assume that both D and H are excited solely by the H Lyman-α line. We have not directly included contributions from the IPM Lyman-α. Table 1 gives a list of the important parameters used in these calculations.

Table 1
Standard parameters used

Parameter	Value
H Lyman-α	1215.67 Å
D Lyman-α	1215.34 Å
πF	4.4×10^{11} photons cm^{-2} s^{-1}
1 sdu[a] = $\Delta\nu_D$ at 500 K	0.0116 Å
x_{off}	18.9 sdu (or 0.219 Å)
x_{dis}	18.5 sdu (or 0.215 Å)
Δ	28.4 sdu (or 0.33 Å)
Oscillator strength, f_{osc}	0.4162
K_h	$2^{+2}_{-1} \times 10^6$ cm^2 s^{-1}

[a] sdu ≡ standard Doppler unit.

2.4. Photochemical model

We follow Parkinson et al. (1999) for the deuterium chemistry of the jovian thermosphere. Table 2 shows the main reactions that we have found to be important. As noted above, jovian H_2 is likely to have effective vibrational temperatures between 1300 and 4000 K excited by fluorescence of sunlight, photoelectron excitation and ion recombination. It is expected that thermospheric HD will be vibrationally excited as well. This follows as the exchange of vibrational quanta between H_2 and HD is almost thermoneutral. Parkinson et al. (1999) have noted that the HD vibrational temperature will be controlled by H_2 via

$$H_2^1 + HD^0 \rightleftharpoons H_2^0 + HD^1 + 0.0651 \text{ eV}, \qquad (R_f,R_r)$$

where k_f and k_r are the rate constants for the forward and reverse reactions, respectively, and the superscripts denote the vibrational level. The production term and loss frequency for HD^1 can be respectively written as

$$P_{HD^1} = k_f[H_2^1][HD^0] \tag{4}$$

and

$$L_{HD^1} = [HD^1]\{k_r[H_2^0] + k_2[H] + k_3[H]\}, \tag{5}$$

Table 2
Deuterium reactions and rate constants

No.	Reaction	Rate constant	Source
(R_f)	$H_2^1 + HD^0 \rightarrow H_2^0 + HD^1 + 0.0651$ eV	See text	a
(R_r)	$H_2^0 + HD^1 + 0.0651$ eV $\rightarrow H_2^1 + HD^0$	See text	a
(R_1)	$H + HD^0 \rightarrow D + H_2^0$	$0.5 \times k_4 \times e^{-413/T}$	a
(R_2)	$H + HD^1 \rightarrow HD^0 + H$	$2.3 \times 10^{-11} e^{-1566/T}$	a
(R_3)	$H + HD^1 \rightarrow H_2^{0,1} + D$	$2.3 \times 10^{-11} e^{-1566/T}$	a
(R_4)	$D + H_2^0 \rightarrow HD^0 + H$	$4 \times 10^{-18} T^{2.29} e^{-2627/T}$	b,c
(R_5)	$D + H_2^1 \rightarrow HD^{0,1} + H$	$2.3 \times 10^{-11} e^{-1566/T}$	d,e,f
(R_6)	$D + CH_3 \rightarrow CH_2D + H$	2.3×10^{-10}	g
(R_7)	$H + CH_2D + M \rightarrow CH_3D + M$	Same as CH_4 production	h,i
(R_8)	$H + CH_2D \rightarrow CH_3 + D$	$1.34 \times 10^{-10} e^{-810/T}$	j
(R_9)	$CH_2D + CH_3 \rightarrow C_2H_5D$	Same as CH_3 self-recombination	h,i
(R_{10})	$C_2H_5 + C_2H_4D \rightarrow C_2H_4 + C_2H_5D$	2.4×10^{-12}	k
(R_{11})	$D + H + M \rightarrow HD + M$	$1.5 \times 10^{-29} T^{-1.3}$	l

[a] See text.
[b] Michael and Fisher (1990).
[c] Mielke et al. (1994).
[d] Dreier and Wolfrum (1986).
[e] Buchenau et al. (1990).
[f] Aoiz et al. (1996).
[g] Seakins et al. (1997).
[h] Romani (1996).
[i] Lee and Yung (2001).
[j] Yung et al. (1988).
[k] Baulch et al. (1992).
[l] We have used the H + H + M rate from Gladstone et al. (1996).

where k_2 and k_3 are the rate constants for

$$H + HD^1 \rightarrow HD^0 + H, \qquad (R_2)$$

$$H + HD^1 \rightarrow H_2^{0,1} + D, \qquad (R_3)$$

respectively. The effect of vibrational quenching of HD by H should be small since $k_{(2+3)}[H] \ll k_r[H_2]$ given that the rate constants k_2 and k_3 are both $\sim 10^{-13}$ cm^3 s^{-1} and $[H] \ll [H_2]$. Hence we can assume the contributions to the loss frequency for reactions (R_2) and (R_3) in Table 2 are small. Hence the density of the first vibrational level of HD can be approximated by

$$\frac{[HD^1]}{[HD^0]} = \frac{k_f}{k_r} \times \frac{[H_2^1]}{[H_2^0]} \qquad (6)$$

$$\approx e^{756/T} \times e^{-5992/T_v} \qquad (7)$$

where T and T_v are respectively the kinetic and an equivalent vibrational temperature for H_2. The ratio of k_f/k_r is given by $\exp(-\Delta G/RT)$, where ΔG is the difference in Gibbs free energy. We approximated ΔG by ΔH, where H is the enthalpy and obtained $k_f/k_r = 0.33$ at 1000 K, which is close to the correct value of 0.38 (Yung and DeMore, 1999, Chapter 3). The results in the paper are not seriously impacted by this approximation. The energy term, H, is determined by the energy difference, ΔE_1, between the vibrational quantum, $v = 1$ for HD and H_2, $k_r = k_f \times e^{-\Delta E_1/(kT)}$, the ratio $[H_2^1]/[H_2^0]$ is obtained from $[H_2^1] = [H_2^0] \times e^{-\Delta E_2/(kT_v)}$, ΔE_2 is the energy difference between energy levels $v = 0$ and $v = 1$ for H_2, and k is Boltzmann's constant in eV (Abgrall et al., 1993). The rate for the forward reaction is $\sim 2.3 \times 10^{-13}$ cm^3 s^{-1} (Buchenau et al., 1990) and so this relationship between $v = 1$ for H_2 and HD should obtain until high in the thermosphere. For our nominal model we choose $T_v = 3T$ and explore other values.

Due to the large densities of H in the jovian thermosphere, the main source of D is given by

$$H + HD^{0,1} \rightarrow H_2^{0,1} + D \qquad (R_1,R_3)$$

with rate constants, k_1 and k_3, respectively. Compared to these sources, CH_3D photolysis to $CH_3 + D$ is minor, but is included in our calculations for completeness. The main loss for D is

$$D + H_2^{0,1} \rightarrow HD^{0,1} + H \qquad (R_4,R_5)$$

with rate constants, k_4 and k_5, respectively. We note that the reactions (R_1) and (R_4) become important for low vibrational temperatures. Since the reactions (R_1) and (R_4) are the reverse of one another we can use detailed balance (Polanyi and Schreiber, 1974) to obtain the rate of reaction k_1 using $k_1/k_4 = 0.5 \times \exp(-413/T)$ where we have simplified the distribution of states by taking the energy difference between the $v = 0$ and $J = 0$ states (Abgrall et al., 1993).

Parkinson et al. (1999) noted that the reaction

$$D + CH_3 \rightarrow CH_2D + H \qquad (R_6)$$

could lead to the formation of deuterated hydrocarbons, in particular, CH_3D via

$$H + CH_2D + M \rightarrow CH_3D + M. \qquad (R_7)$$

Some of the CH_3D is expected to photolyze to yield CH_2D + H since the CH bond is weaker than the CD bond (cf. Seakins

et al., 1997). This infusion of the D into hydrocarbons will fuel the formation of higher order deuterated species and was recently investigated by Lee and Yung (2001) who looked at the formation of CH_3D and C_2H_5D in detail. The authors of Lee and Yung (2001) pointed out that Parkinson et al. (1999) had omitted the important reverse reaction to (R_6)

$$H + CH_2D \rightarrow D + CH_3, \quad (R_8)$$

which plays an significant role in reducing the formation of deuterated hydrocarbons. We have included this reaction along with the other reactions cited in Lee and Yung (2001) involving the formation of deuterated hydrocarbons. The main C_2H_5D reactions are

$$CH_2D + CH_3 \rightarrow C_2H_5D \quad (R_9)$$

and

$$C_2H_5 + C_2H_4D \rightarrow C_2H_4 + C_2H_5D. \quad (R_{10})$$

Lee and Yung (2001) did not include the effect of vibrational temperature in their discussion of deuterated hydrocarbons which we have included here.

We have also included the relatively unimportant reaction

$$H + D + M \rightarrow HD + M \quad (R_{11})$$

as an additional sink for D.

The top of the chemical model is within the ionosphere. The ion molecule reactions that generate H have not been included directly in the chemical model. Rather, the impact of the ionosphere has been allowed for by adopting a downward flux, $\phi_{top}(H)$ at the top of the model. H is produced by ionization of H_2 by photons and photoelectrons,

$$H_2 + h\nu \rightarrow H_2^+ + e, \quad (8)$$

$$H_2 + e \rightarrow H_2^+ + 2e, \quad (9)$$

followed by reaction with H_2 to produce H_3^+

$$H_2^+ + H_2 \rightarrow H_3^+ + H \quad (10)$$

and recombination of H_3^+

$$H_3^+ + e \rightarrow 3H \quad (11)$$

or

$$H_3^+ + e \rightarrow H + H_2. \quad (12)$$

In our case, we assume that every photon gives rise to four H atoms. For solar maximum EUV fluxes capable of ionizing H_2 this would imply a minimum H source of about 4×10^9 H atoms $cm^{-2}\,s^{-1}$ at Jupiter (e.g., Gladstone et al., 1996). However, to obtain the assumed H column of $\sim 3.7 \times 10^{17}$ cm^{-2} above the CH_4 absorbing layer to provide the Lyman-α airglow, we find it necessary to supply an H flux of 15×10^9 $cm^{-2}\,s^{-1}$ at the top of the model for our standard reference temperature profile and 12×10^9 $cm^{-2}\,s^{-1}$ for the Romani temperature profile, which fall within the range of values tested by Gladstone et al. (1996). It is assumed that the H flux coming from the ionosphere implies a concomitant D flux, $\phi_{top}(D)$, which is estimated by scaling the H flux by the HD mixing ratio at the top of the model divided by 2. Thus, we adopt $\phi_{top}(D) = 0.5\phi_{top}(H)\,f_{HD}$ as a standard, where f_{HD} is the HD/H_2 mixing ratio at the model top. Well below the homopause at the bottom of our model atmosphere, we assume that D and H are in photochemical steady state (PCSS) since the chemical time constant is much shorter than that for diffusion which we discuss later. As noted above it is necessary to have a realistic H distribution which we have obtained using measurements to constrain the H distribution in the thermosphere. This is done by adjusting $\phi_{top}(H)$ to give the column H that satisfies the H Lyman-α constraint. The H distribution is provided by the photochemical diffusion model, which shows some sensitivity to the temperature profile.

The species densities shown in this paper were calculated by solving the continuity equation for each species, i,

$$\frac{\partial n_i}{\partial t} + \frac{\partial \phi_i}{\partial z} = P_i - L_i, \quad (13)$$

where the vertical flux, ϕ_i, is given by

$$\phi_i = \phi_i^K + \phi_i^D. \quad (14)$$

The eddy flux, ϕ_i^K,

$$\phi_i^K = -K\left(\frac{\partial n_i}{\partial z} + \left(\frac{1}{H_{av}} + \frac{1}{T}\frac{\partial T}{\partial z}\right)n_i\right) \quad (15)$$

represents the vertical flux that parameterizes macroscopic motions, such as the large scale circulation and gravity waves, while ϕ_i^D

$$\phi_i^D = -D_i\left(\frac{\partial n_i}{\partial z} + \left(\frac{1}{H_i} + \frac{(1+\alpha_i)}{T}\frac{\partial T}{\partial z}\right)n_i\right) \quad (16)$$

is the vertical flux as a result of molecular diffusion. The species number density is given by n_i, P_i is the chemical production rate ($cm^{-3}\,s^{-1}$) and L_i is the loss rate ($cm^{-3}\,s^{-1}$) at altitude z and time t (e.g., Chamberlain and Hunten, 1987). D_i and K are respectively the molecular and eddy diffusion coefficients. The species and atmospheric scale heights are denoted by H_i and H_{av}, respectively. In these calculations we have neglected the effects of the thermal diffusion factor, α_i, as its inclusion contributed less than 1% to the deuterium column in test runs.

The photochemical model used for these calculations contains reactions involving H, D, CH_x, CH_xD, C_2H_x, C_2H_xD, and C_2. Additional reactions involving higher order hydrocarbons of the form C_3H_x and C_4H_x have not been included here for simplicity since the main focus of this study is deuterium Lyman-α and they should have little impact. As the model has not been formally presented before, the details are given in Appendix A.

2.5. Radiative transfer

Parkinson et al. (1999) applied a resonance scattering model to the D + H problem that uses the Feautrier technique to solve the coupled equations of radiative transfer (Griffioen et al., 1994; Griffioen, 2000) and for the uncoupled H and D cases

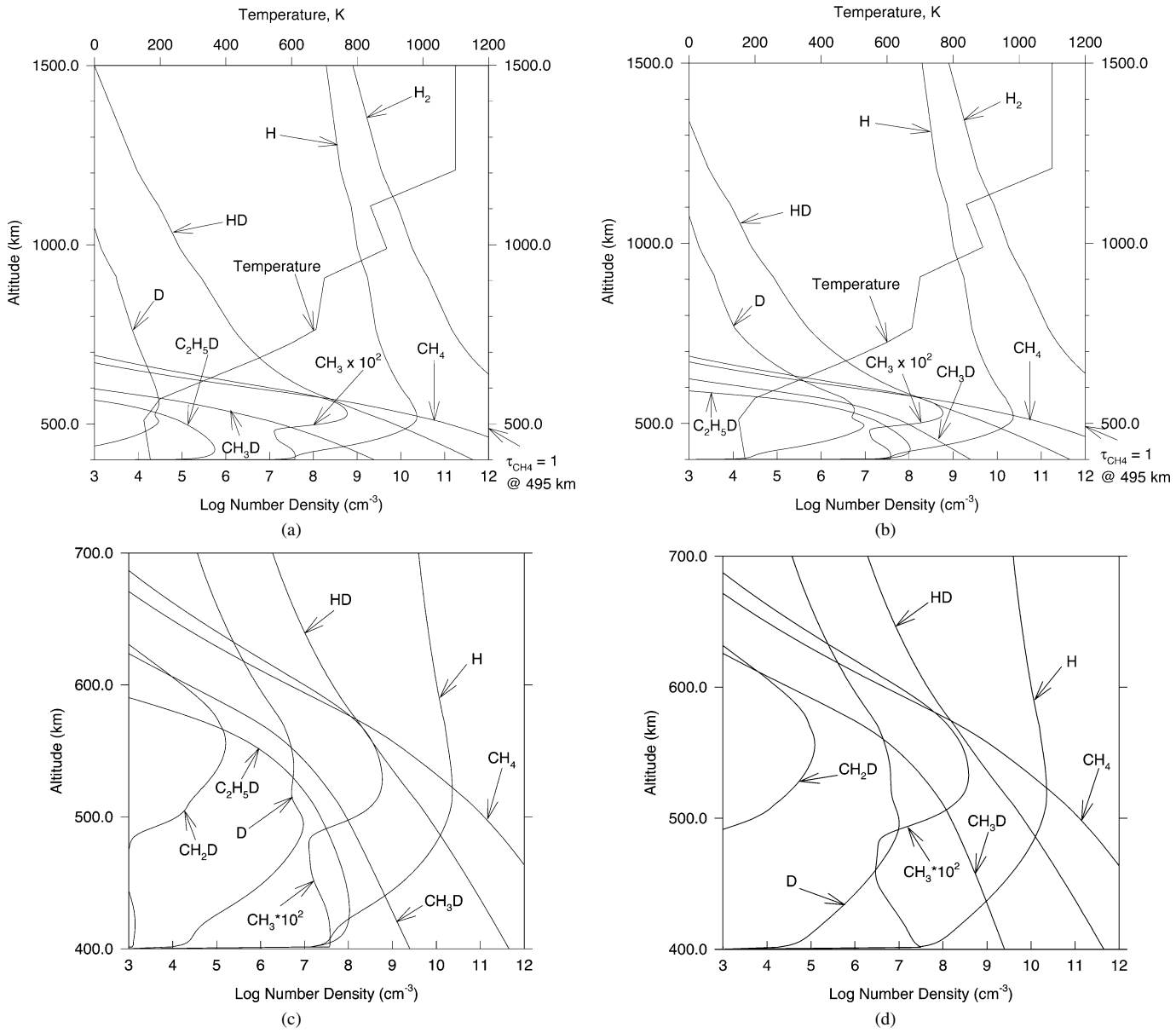

Fig. 2. The model atmospheres of some of the more relevant species considered, viz., H_2, CH_4, CH_3, CH_2D, CH_3D, C_2H_5D, HD, H, and D. (a) The neutral temperature profile corresponding to Seiff et al. (1997) (viz., $T_v = T$) was used. (b) The standard reference temperature profile with $T_v = 3T$ was used. (c) Close up of (b) for the altitude range 400–700 km, corresponding to the scattering region. (d) Similar to (c) except it includes a modified $H + CH_3 \rightarrow CH_4$ reaction rate suggested by Lee et al. (2000), Moses et al. (2000) as described in the text and C_2H_5D omitted. (e) Similar to (c) except comparing D, CH_3D, and C_2H_5D number density profiles for $T_v = 3T$ for Seiff et al. (1997) and Romani (1996) neutral temperature profiles.

for subsolar conditions (Griffioen et al., 1994; Griffioen, 2000; Gladstone, 1982).

Methane is the main absorber of H and D Lyman-α photons in Jupiter's atmosphere. The level where the CH_4 optical depth, τ_{CH_4}, is unity is dependent upon the value of the eddy diffusion coefficient at the homopause, K_h. The altitude where the $\tau_{CH_4} = 1$ is important since it is a measure of where in the atmosphere the majority of these photons will be absorbed. Hence, all of the scattering of H and D Lyman-α photons will occur above $\tau_{CH_4} \leqslant 1$ and we refer to this part of the atmosphere as the 'scattering region' for deuterium. We also note that a dense altitude grid will be required for radiative transfer calculations at $\tau_{CH_4} \sim 1$ since the D number density has a large increase for a small change in altitude.

3. Results and discussion

In earlier sections, we have described a photochemical model to define a standard reference model atmosphere and a radiative transfer model to describe the emission of deuterium in the jovian upper atmosphere. Using these models, we now report on the effects of varying important parameters in relation to a standard reference atmosphere and how this impacts the deuterium distribution and the H and D Lyman-α airglow in thermosphere.

Fig. 2a contains a plot illustrating the key species, viz., H_2, CH_4, CH_3, CH_2D, CH_3D, C_2H_5D, HD, H, and D in a model atmosphere where the neutral temperature profile (Seiff et al., 1997) has been used with $T_v = T$. Fig. 2b shows the

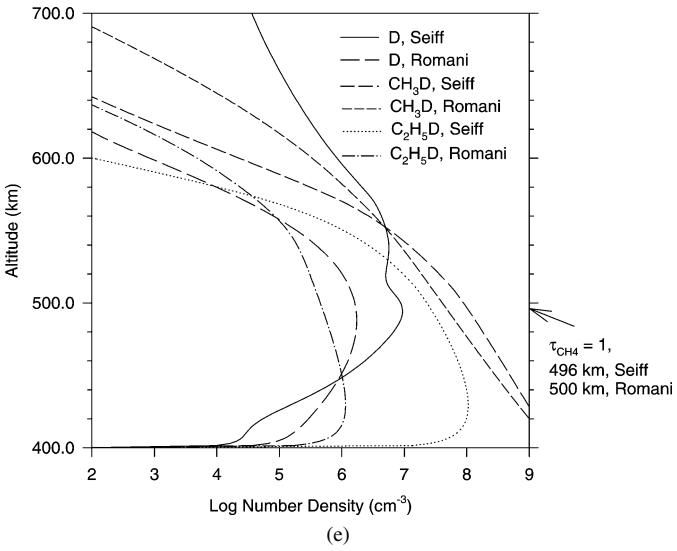

(e)

Fig. 2. (*continued*)

same species, except that $T_v = 3T$, which is the standard reference T_v used in the photochemical modeling. The D profiles shown in Figs. 2a and 2b have total D column amounts of 6.9×10^{11} and $\sim 7.4 \times 10^{13}$ cm^{-2}, respectively. The CH_3 profile mainly results from production via photolysis of CH_4, and loss due to self-recombination and reaction with H. Fig. 2c is a more detailed presentation of the results in Fig. 2b. Comparing Figs. 2a and 2b, it is clear that the vibrational temperature of H_2 can significantly affect the amount of deuterium in the thermosphere.

Fig. 2d shows the same profiles as in Fig. 2c, except now we have used the faster $H + CH_3 \rightarrow CH_4$ reaction rate constant suggested by Moses et al. (2000) and Lee et al. (2000) for comparative purposes (cf. Table 3).

As expected, a comparison between Figs. 2c and 2d shows a decrease in the overall CH_3 profile due to the faster reaction rate which corresponds to a ∼33% decrease in the CH_3 column density. Since we use the same reaction rate constant, k_6, there is also a slight change D profile corresponding to a slight net increase in column D above $\tau_{CH_4} = 1$. Lee and Yung (2001) suggests changes in the reaction rate constant k_7 that strongly influence the D abundance, but other changes in C_2 chemistry by those authors produce negligible variation in the results from these calculations.

Fig. 2e gives a comparison of the resultant D, CH_3D, and C_2H_5D number density profiles for $T_v = 3T$ for the GPMS (Seiff et al., 1997) and Romani (1996) neutral temperature profiles shown in Fig. 1a. Since the GPMS temperature profile is hotter, we expect the GPMS D column in the scattering region to be greater than the corresponding Romani case. The GPMS D column is about 4.8×10^{13} atoms cm^{-2} above $\tau_{CH_4} = 1$, greater than the Romani D column by a factor of ∼20 and hence will result in a brighter D Lyman-α emission. The corresponding CH_3 column in the scattering region decreases by a factor of ∼1.5 to 3.1×10^{13} atoms cm^{-2} over the Romani case results. Clearly an increase in the neutral temperature profile (and subsequently the vibrational temperature profile) causes a much greater change in the D column in the deuterium scattering region than does the changing the reaction rate for reaction (k_6) (Moses et al., 2000; Lee et al., 2000). We also see from the figure that the cooler temperature profile results in significant decreases in the CH_3D and C_2H_5D number density profiles.

Figs. 3a–3d are plots showing how varying T_v affects the key species considered. Fig. 3a shows the D profiles resulting from calculations using the vibrational temperature profiles shown in Fig. 1b. The D profiles corresponding to the various T_v's exhibit 'similar' behavior with altitude and the D column above $\tau_{CH_4} = 1$ (given in Table 4) increases from about 6.4×10^{11} to 2.2×10^{14} atoms cm^{-2} for increasing n (recalling $T_v = nT$). The fraction of the total deuterium column below $\tau_{CH_4} = 1$ increases as n gets larger and for $T_v = 3T$, only ∼70% of the deuterium is located above the $\tau_{CH_4} = 1$ level. We discuss this in more detail later in the paper.

We see in Fig. 3a that as T_v increases from T to $2T$, there is little change in the D profile since there is a low concentration of vibrationally excited species produced for this low value for T_v. However, when higher values of T_v are considered larger changes in the D profile obtain. This is due to the large activation energies for reactions (R_2) and (R_3). The D number density is much larger everywhere below ∼580 km for $n \geqslant 2.5$, increasing with increasing n and having a maximum occurring right at the $\tau_{CH_4} = 1$ level. This is because the reaction rates (cm^3 s^{-1}) governing the D production become faster with increasing vibrational temperature. However, increasing the vibrational temperature has little effect on the CH_3 profile as we see in Fig. 3b. Where does this D come from? The source is HD which becomes increasingly depleted as $T_v = nT$ increases, as shown in

Table 3
Rate constants for modified CH_3 chemistry[a]

Rate	High-pressure rate constant, k_∞	Low-pressure rate constant, k_0
k_A, $CH_3 + CH_3 \rightarrow C_2H_6$ [b,c]	$1.5 \times 10^{-7} T^{1.18} e^{-329/T}$	$8.76 \times 10^{-7} T^{-1.18} e^{-329/T}$
k_B, $CH_3 + CH_3 \rightarrow C_2H_6$ [b,d]	6.0×10^{-11}	$1.8 \times 10^{-16} T^{-3.75} e^{-300/T}$
k_C, $H + CH_3 \rightarrow CH_4$ ($T > 296$ K) [b,d,e]	–	$2.3 \times 10^{-17} T^{-4.03} e^{-1366/T}$
k_C, $H + CH_3 \rightarrow CH_4$ ($T < 296$ K) [b,d,e]	–	$1.4 \times 10^{-19} T^{-3.75} e^{-300/T}$

[a] Two-body rate constants are in units of cm^3 s^{-1} while the three-body rate is in cm^6 s^{-1}.
[b] See text.
[c] Slagle et al. (1988).
[d] Lee et al. (2000).
[e] Moses et al. (2000).

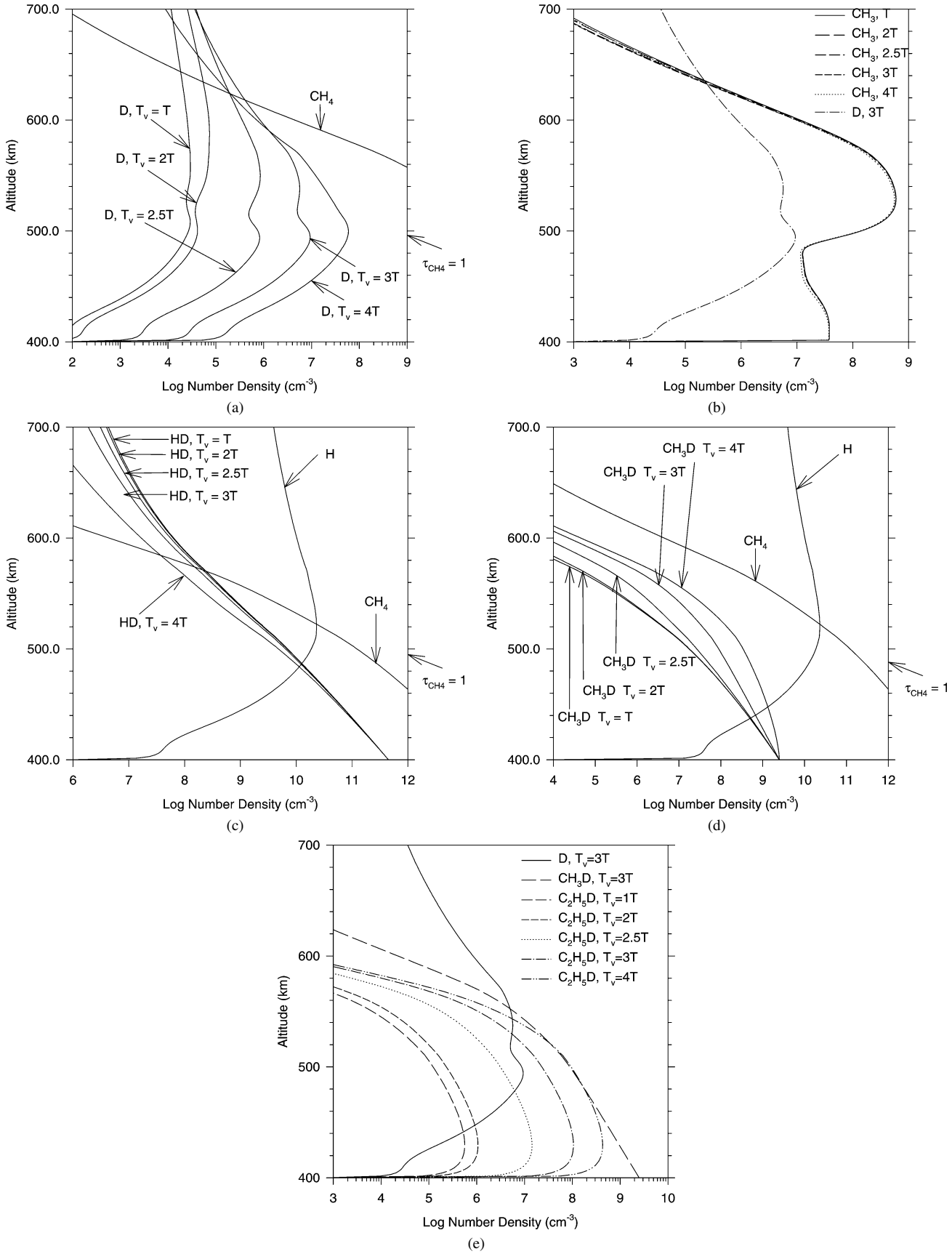

Fig. 3. Various D (a), CH_3 (b), HD (c), CH_3D (d), and C_2H_5D (e) profiles resulting from calculations utilizing vibrational temperature profiles corresponding to $T_v = nT$, where $n = 1, 2, 2.5, 3$, and 4. Since H is constrained, the H and CH_4 profiles are not sensitive to T_v (c and d). Hence, only one profile for these species is plotted.

Table 4
Column D comparison

T_v	D column (cm^{-2}) above $\tau_{CH_4} = 1$	Total D column (cm^{-2})	Fraction of D in scattering region	Disk brightness (subsolar case) (R)
$1T$	6.4×10^{11}	6.9×10^{11}	0.93	50
$2T$	1.4×10^{12}	1.5×10^{12}	0.93	120
$2.5T$	8.6×10^{12}	1.1×10^{13}	0.78	430
$3T$	5.0×10^{13}	7.4×10^{13}	0.68	760
$4T$	2.2×10^{14}	3.5×10^{14}	0.63	880

Fig. 3c. Some of this increase of D is used in the fast production of CH_2D via reaction (R_6) which in turn is converted to CH_3D, C_2H_5D and other deuterated species. Additionally, for decreasing CH_3 at lower altitudes, with increasing K_h, there is less photolysis since $\tau_{CH_4} = 1$ level moves higher in altitude.

Figs. 3d and 3e respectively show plots of the deuterated methane and ethane profiles for various $T_v = nT$. Most of the production of these two species, both of which increase with increasing T_v, occurs between ~480 to 600 km, flow down to the lower boundary resulting in their enhanced mesospheric mixing ratios. For example, at 500 km CH_3D and C_2H_5D are respectively enhanced by a factor of ~5 and ~200 for $T_v = 3T$ and ~20 and ~700 for $T_v = 4T$. This suggests that if CH_3D and C_2H_5D could be measured in this height region, a sensitive indicator of T_v would obtain. The amount of CH_3D in Fig. 3d is not as much as that shown from calculations by Parkinson et al. (1999): this is directly attributable to reaction (R_8) for which a substantial amount of the CH_3D reverts to CH_2D. We note since column H is being constrained in our calculations, the H and CH_4 profiles are not very sensitive to T_v and so one plot only for these species is shown in Figs. 3c and 3d.

Figs. 4a–4d are plots showing how the variation of K_h affects the key species considered. Fig. 4a shows the number density profiles for D, HD, and CH_4 for various K_h given

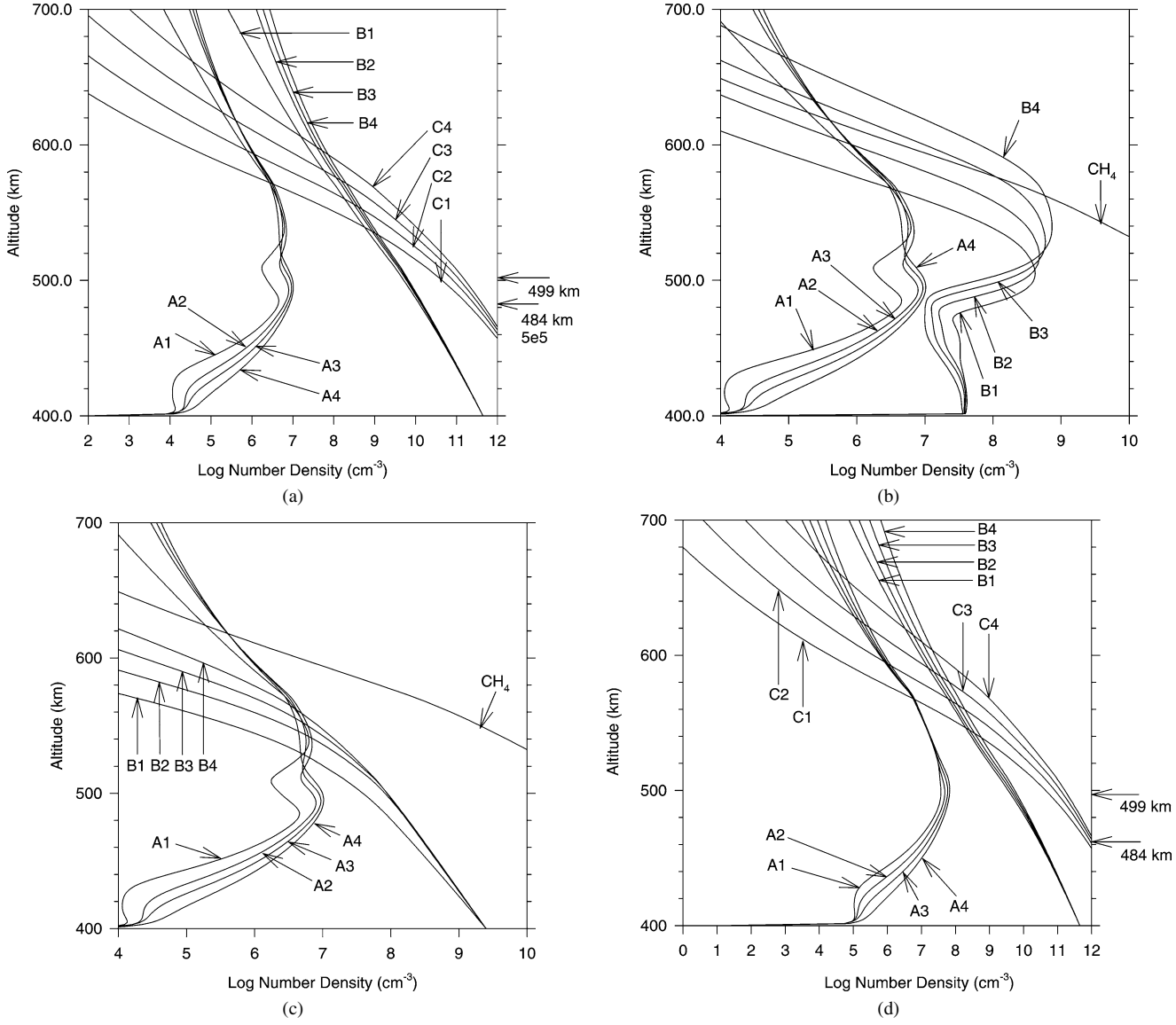

Fig. 4. Density profiles for various K_h and $T_v = 3T$: (a) D (A), HD (B), and CH_4 (C); (b) D (A) and CH_3 (B); (c) D (A) and CH_3D (B). (d) Same as (a) except $T_v = 4T$. The labels 1, 2, 3, and 4 refer to $K_h = 5 \times 10^5$, 10^6, 2×10^6, and 4×10^6 $cm^2\,s^{-1}$, respectively.

$T_v = 3T$, which indicates minimal impact of increasing K_h on HD. Since by definition, the methane homopause is determined by $K_h = D$, the CH_4 profiles are included in Fig. 4a. As expected, we see that increasing K_h increases the column amount of CH_4 in the scattering region, since both HD and CH_4 are carried higher in the atmosphere with increasing K_h. The arrows and height markings on the right-hand side of the graph indicate the range for the $\tau_{CH_4} = 1$ level for the CH_4 profiles included.

The variation of K_h has a modest impact the D profiles in the scattering region. Varying K_h by a factor of two ($K_h = 2^{+2}_{-1} \times 10^6$ cm^2 s^{-1}) while keeping the H column fixed, we find that the D column varies by less than ~40% for a fixed T_v above $\tau_{CH_4} = 1$. For K_h between these values, the D column density is fairly constant above $\tau_{CH_4} = 1$. Fig. 4b shows the variation of D and CH_3 for various K_h, $T_v = 3T$. In the scattering region, increasing K_h results in increasing CH_3 since CH_3 is mainly derived from CH_4 in this region. Below the scattering region, increasing K_h results in decreasing CH_3. This is because there is more H available (at these levels) and reaction of CH_3 with H becomes more dominant in this mixed region well below the homopause (at ~560 km).

Fig. 4c shows D and CH_3D for various K_h, $T_v = 3T$. We see that CH_3D increases for increasing values of K_h because it is transported higher up in the scattering region with more vigorous mixing. Figs. 4b and 4c show only the CH_4 profile for the standard reference K_h and $T_v = 3T$ for clarity.

Fig. 4d shows the same species as Fig. 4a except that $T_v = 4T$. As we saw in Fig. 4a, the column D is not significantly increased in the scattering region as a function of increasing K_h. The arrows on the right-hand side of the figure are analogous to those for Fig. 4a.

In Fig. 5 we examine the H and D columns above $\tau_{CH_4} = 1$ for various H_2 vibrational temperature profiles as a function of eddy diffusion coefficient at the homopause: fixed H and D fluxes are introduced at the upper boundary. As expected, for a fixed H flux at the upper boundary, we see that in all cases the H column densities decrease for increasing K_h. As we saw earlier, the D column is minimally affected by a change in K_h (cf. Figs. 4a and 4d).

Figs. 5a and 5b also show that increasing T_v makes little change to the column H and increases the column D independent of K_h. Fig. 5b also shows that the column amounts of deuterium are very sensitive to the vibrational temperature profiles when the H flux is held constant for each K_h (cf. Fig. 5a).

As noted above we have selected an H column density of $\sim 3.7 \times 10^{17}$ cm^{-2} as our standard reference to match the constrained column H value given by Ben Jaffel et al. (1993). In order to obtain this value for the column H in our model, it is necessary to adjust the input H flux, Φ_H, at the model atmosphere upper boundary. For the standard model we require $\Phi_H = 15 \times 10^9$ cm^{-2} s^{-1}, but we have also considered the values $\frac{1}{15}\Phi_H$, $\frac{1}{3}\Phi_H$, $\frac{2}{3}\Phi_H$, and $\frac{4}{3}\Phi_H$ for comparative purposes. Higher values for Φ_H may be interpreted as having a component of the H column being due to transport of H from auroral regions or possibly (to a much lesser extent) from the production of local electrons (Wong et al., 2003; Waite et al., 1983; McConnell et al., 1982; Broadfoot et al., 1981; Yung and Strobel, 1980).

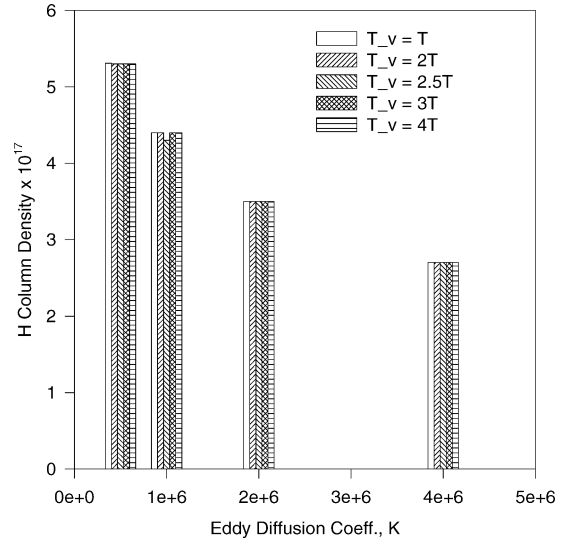

(a)

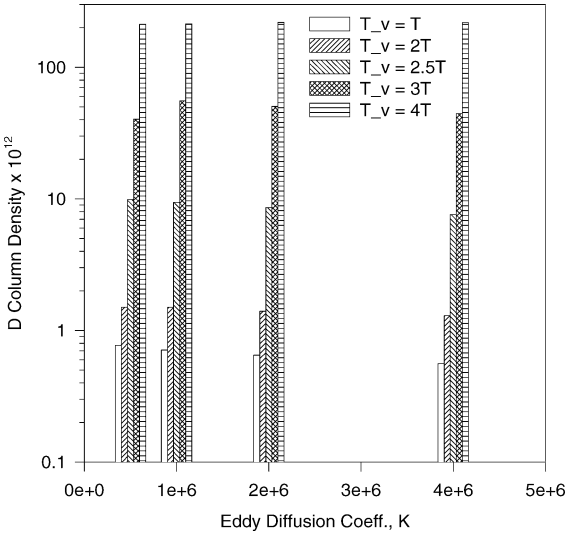

(b)

Fig. 5. Column H and D as a function K_h; for the standard reference temperature profile and several values of T_v: H (a) and D (b) column density versus Eddy diffusion coefficient K. All cases are for columns above $\tau_{CH_4} = 1$.

Φ_D was held fixed to the standard reference value while altering Φ_H to see the effect of changing the column H value only. Calculated D and H profiles corresponding to varying the H column density are shown in Fig. 6. As expected, an increase in the H flux increases the amount of H with altitude which subsequently causes a linear increase in the D profile. Thus, over the range of H flux values we have selected, the deuterium number density profile increases by about an order of magnitude for a similar change in the H flux which is relatively minimal when compared with the variation of D as a function of T_v.

We now look at the impact of uncertainties in the HD mixing ratio, f_{HD}, at the model atmosphere lower boundary. f_{HD} was varied about the standard reference value to include the tightly constrained upper and lower extremes of the error bars on the GPMS measurement analysis by Mahaffy et al. (1998). As expected, increasing HD increases both D and CH_3D. The calculated D, HD, and CH_3D profiles are given in Fig. 7. Here

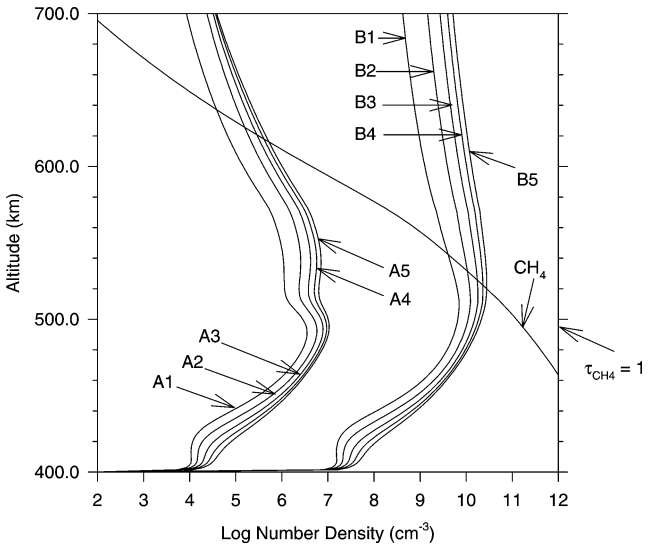

Fig. 6. Calculated D (A) and H (B) profiles corresponding to varying the input H flux, Φ_H at the model atmosphere upper boundary. The labels 1, 2, 3, 4, and 5 refer to $\Phi_H = 1 \times 10^9$, 5×10^9, 10×10^9, 15×10^9, and 20×10^9 cm^{-2} s^{-1}, respectively.

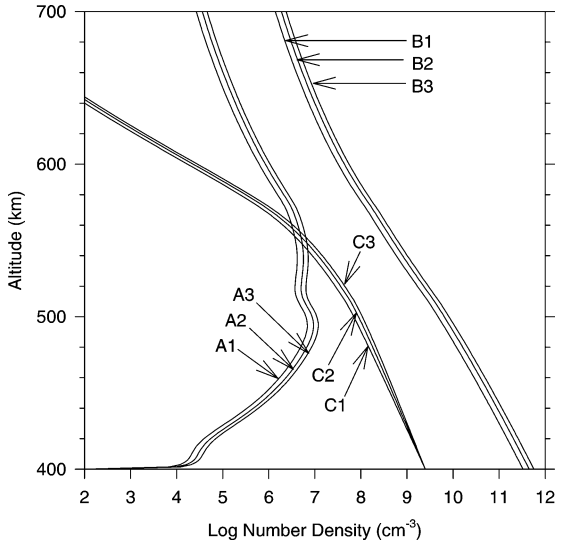

Fig. 7. Calculated D (A), HD (B), and CH_3D (C) profiles corresponding to changes in HD mixing ratio at the model atmosphere lower boundary, f_{HD}. The labels 1, 2, and 3 refer to $f_{HD} = 3.3 \times 10^{-5}$, 4.5×10^{-5}, and 5.7×10^{-5}, respectively.

we see that any increase in f_{HD} in the scattering region produce linear increases in the D profile, and nearly linear increases in the CH_3D profiles.

Regions where the chemical time constant, $\tau_c = (\delta L_i / \delta n_i)^{-1}$, is shorter than the diffusion time constant tells us where the atmosphere is in PCSS and where chemical processes are dominant. Fig. 8 shows various time constants for the standard reference atmosphere. Depicted are τ_c for both D and HD and the diffusion time constant $\tau_{diff} = H_{ave}^2/(D + K)$ versus height for just D. For D and HD the chemical time constants are longer than the diffusion time constant above 1750 and 1500 km, respectively. Thus they are both, to a close approximation, in diffusive equilibrium above these heights. This is also the case

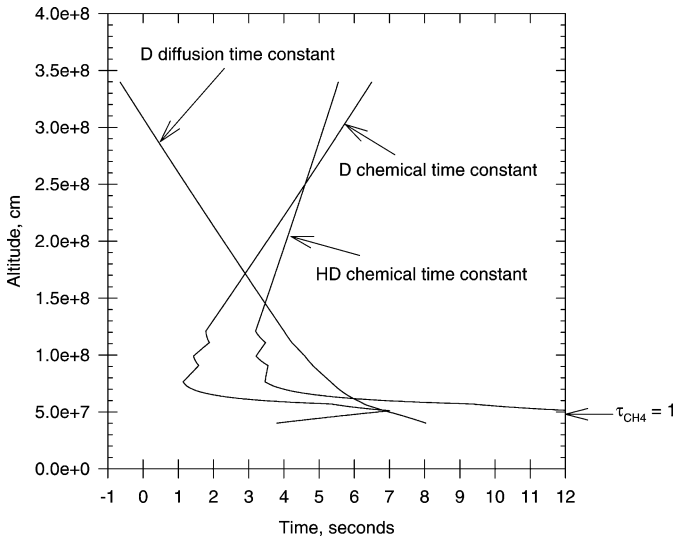

Fig. 8. Chemical and diffusion time constants for D and HD, τ_D, τ_{HD}, τ_{diff}.

for HD below 700 km, which is the region of interest in our study of deuterium. However, for D, below 1750 km, chemical time constants are shorter and so PCSS is an adequate approximation in the region of interest.

An investigation into the effect of the location of the 'hot' H region versus altitude was carried out and showed little impact on the results. The way we proceeded was to initially locate the 'hot' region at the top of the atmosphere and then adjust it downwards until the bottom of the region was located at about 1900 km. Below this altitude, the 'hot' region is presumed to not be sustainable due to a high collision rate owing to increasing n_{H_2} (Parkinson, 2002). In addition, halving or doubling the column amount of 'hot' H changed the D Lyman-α brightness by less than 7%. This was expected since most of the deuterium is much lower in the atmosphere than where the 'hot' H resides. Since the inclusion of a 'hot' region is seen to minimally affect all calculations, no figures have been included regarding this parameter.

The standard reference atmosphere adopted in this work uses the CH_4 and HD mixing ratios from the GPMS experiment which are different from those used by Parkinson et al. (1999). The higher CH_4 mixing ratio and slightly lower HD mixing ratio results in a reduced D concentration overall and lower D Lyman-α emergent intensities for the various cases given the same conditions. Fig. 9a shows the total intensities of the H and D lines across the disk of Jupiter for conditions for which the solar zenith angle, SZA = viewing angle and $T_v = 3T$. At the subsolar point the total H intensity is ~12.5 kR while that of D is ~700 R. This result (using our standard model atmosphere with $T_v = 3T$) does not violate the ~500 R upper limit for D Lyman-α that we estimate from the H Lyman-α observations taken in the vicinity of the bulge region on the disk of Jupiter using the HST Goddard High Resolution Spectrograph (GHRS) (Emerich et al., 1996). Fig. 9b shows the same profiles as those shown in Fig. 9a, but focusing on the vicinity of the D Lyman-α line for various locations across the disk for $T_v = 3T$. Comparing this figure with its analogue in Parkinson et al. (1999), it is still seen that although the H Lyman-α is limb darkened

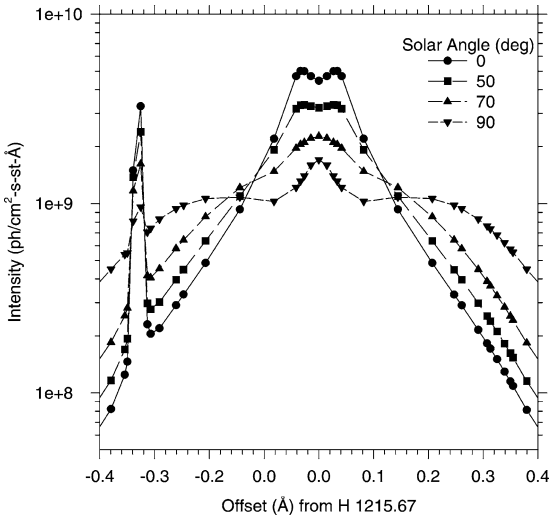

(a)

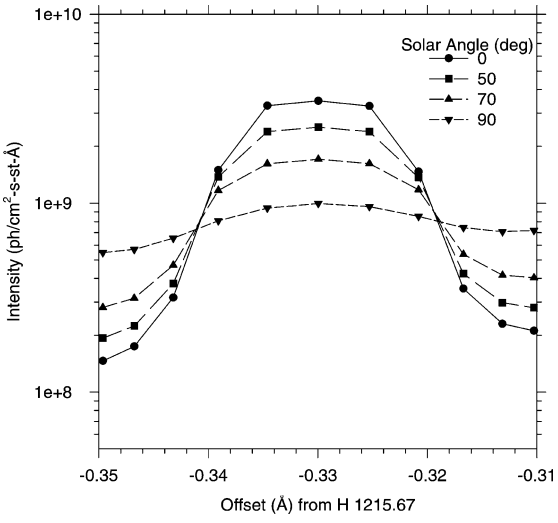

(b)

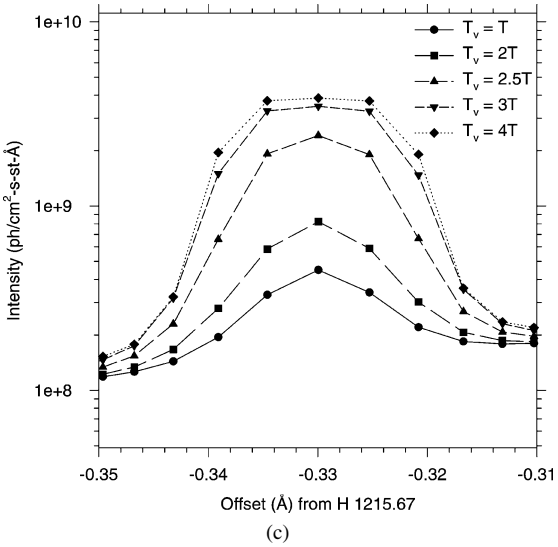

(c)

Fig. 9. (a) H and D Lyman-α intensity profiles for several solar zenith angles with the same viewing angle (i.e., SZA = viewing angle) for the standard reference atmosphere, (b) same as (a) except close up of D Lyman-α intensity profiles at ∼0.33 Å offset from H at 1215.67 Å, (c) close up of D Lyman-α intensity profiles at ∼0.33 Å offset from H at 1215.67 Å for subsolar case for various $T_v = nT$.

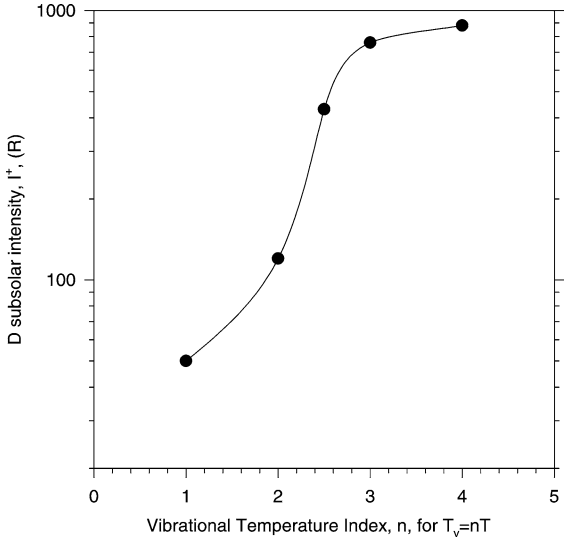

Fig. 10. D Lyman-α subsolar intensities as a function of vibrational temperature.

in the line core it is limb brightened in the wings. Since the D Lyman-α is also limb darkened the contrast between D and H Lyman-α is most noticeable at subsolar locations according to our model. This is in contrast to the original assertion by Ben Jaffel et al. (1998), who claimed that D emissions should be limb brightened owing to the assumption that D is optically thin.

For terminator viewing conditions the predicted D maximum total intensity value is ∼150 R for the maximum D column (cf. Parkinson et al., 1999). For these reasons, we restrict the remainder of the radiative transfer calculations in this study to the subsolar case only.

Fig. 9c shows the combined H and D Lyman-α line profiles for the subsolar case (overhead sun and viewing) for various $T_v = nT$. The D column amount increases with increasing vibrational temperature as listed in Table 4, and the corresponding D emergent intensities are 50, 120, 430, 760, and 880 R, respectively (cf. Fig. 10). This is expected when we compare Fig. 9c with Fig. 3a since there is generally more D available with increasing vibrational temperature, $T_v = nT$. The amount of D above 580 km falls off more rapidly for increasing n and the more significant contribution to the column D for $T_v = nT$ for larger n in the scattering region comes from the peak in D number density that occurs at and just above $\tau_{CH_4} = 1$.

A comparison of emergent D Lyman-α emission is made between the following scenarios: (a) the standard reference case, (b) the standard reference case except using temperature profile A (Romani, 1996) instead of the GPMS temperature profile (Seiff et al., 1997), (c) the standard reference case using the suggested rate for reaction (k_6) given by Lee et al. (2000) and Moses et al. (2000). For these cases the emergent D Lyman-α emissions are (a) 760 R, (b) 880 R, and (c) 770 R, respectively. Hence, an atmosphere with a hotter thermosphere such as temperature profile A can result in a brighter emergent D Lyman-α emission, whereas changing the rate constant for reaction (R_6) has little or no effect on the D emission.

4. Conclusions

Jupiter's D abundance appears to be primarily governed via production by reaction of H with vibrationally hot HD and loss by reaction of D with $H_2^{0,1}$ and CH_3. Below 540 km, removal of D by CH_3 transfers D to deuterated hydrocarbons. The D Lyman-α emission due to D abundances can be seen quite clearly on the wings of the H line and we note that subsolar viewing will provide much better observations since the D Lyman-α is limb darkened and the best contrast between D and H Lyman-α is most noticeable at subsolar locations.

Modeling that incorporates the jovian bulge region has little impact on the deuterium abundance when compared to non-bulge calculations since most of the deuterium is lower in the thermosphere. We have found that a warmer neutral temperature profile in the lower thermosphere increases the deuterium abundance in the scattering region and subsequently results in a brighter jovian D emission by about 15% when compared to the reference case. Increasing the vibrational temperature above $T_v = 2.5T$ causes dramatic increases in the deuterium abundance above $\tau_{CH_4} = 1$ for all cases. The CH_3D and C_2H_5D columns increase with increasing vibrational temperature. The CH_3D and C_2H_5D profiles are enhanced in the lower thermosphere due to the source of deuterated non-methane hydrocarbons in the mesosphere. Higher vibrational temperature profiles, viz. $T_v = 4T$ or greater, are expected in auroral regions which should result in brighter D Lyman-α airglow at these latitudes. However, since K_h should be stronger at higher latitudes (Sommeria et al., 1995), which would affect the D Lyman-α emissions in the opposite way, brighter D Lyman-α airglow may not obtain.

After vibrational temperature, eddy mixing, atomic H flux and the HD mixing ratio are the next most important parameters in our calculations. While K_h does not significantly affect D in the scattering region, the column amount for CH_3D and C_2H_5D increases with increasing K_h. Changing the atomic H flux at the upper boundary of the atmosphere causes minimal changes in the D profile for all but the lowest value considered for this parameter. Additionally, the HD mixing ratio is tightly constrained by the GPMS values calculated by Mahaffy et al. (1998), and so varying this parameter within the error bars given does not dramatically affect the D column in the scattering region. Hence, the small differences in the D profiles resulting from any changes in both of these parameters will not seriously affect the D Lyman-α airglow.

The rate constants for the main CH_3 loss reactions are still uncertain at present, with the exception of the recent result of Cody et al. (2003) for the self-recombination of CH_3. However, allowing for maximal differences in the CH_3 column due to reaction with H causes a negligible difference in the D Lyman-α airglow when compared with the reference case.

This paper concerns studies of the thermosphere of Jupiter with the aim of achieving a better understanding of some aspects of the chemistry and airglow of deuterated species. What

Table 5
Integrated solar flux at 1 AU and cross sections[a]

λ (Å)[b]	Integrated flux[c]	H_2[d]	CH_4[e]	C_2H_2[f]	C_2H_4[e]	C_2H_6[g]
1000	6.2(9)	0.0	3.6(−17)	2.7(−17)	5.0(−17)	5.0(−17)
1050	6.2(9)	0.0	3.0(−17)	2.5(−17)	4.0(−17)	4.7(−17)
1100	1.2(9)	0.0	2.2(−17)	2.5(−17)	1.9(−17)	4.0(−17)
1150	1.9(9)	0.0	1.8(−17)	1.4(−17)	1.6(−17)	3.0(−17)
1200	1.4(10)	0.0	1.9(−17)	1.4(−17)	2.2(−17)	2.2(−17)
1216	4.4(11)	0.0	1.6(−17)	2.8(−17)	2.5(−17)	2.0(−17)
1250	6.7(9)	0.0	1.8(−17)	1.5(−17)	2.8(−17)	2.1(−17)
1300	2.5(10)	0.0	1.7(−17)	6.3(−17)	1.7(−17)	1.8(−17)
1350	1.4(10)	0.0	7.2(−18)	3.0(−17)	2.0(−17)	1.1(−17)
1400	1.8(10)	0.0	1.1(−18)	4.0(−18)	1.3(−17)	6.7(−17)
1450	2.7(10)	0.0	2.2(−20)	1.0(−17)	1.1(−17)	2.4(−18)
1500	5.2(10)	0.0	8.9(−23)	3.0(−17)	1.8(−17)	9.4(−19)
1550	7.1(10)	0.0	8.8(−24)	5.6(−19)	2.4(−17)	9.8(−20)
1600	9.7(10)	0.0	6.0(−24)	6.7(−19)	3.0(−17)	1.1(−21)
1650	2.1(10)	0.0	0.0	9.3(−19)	3.6(−17)	0.0
1700	3.7(11)	0.0	0.0	1.2(−18)	2.6(−17)	0.0
1750	6.3(11)	0.0	0.0	1.1(−18)	1.5(−17)	0.0
1800	8.3(11)	0.0	0.0	7.4(−19)	1.6(−18)	0.0
1850	1.3(12)	0.0	0.0	3.7(−19)	3.7(−19)	0.0
1900	1.9(12)	0.0	0.0	1.5(−19)	5.0(−20)	0.0
1950	2.6(12)	0.0	0.0	1.1(−19)	1.0(−20)	0.0
2000	3.4(12)	0.0	0.0	5.0(−20)	1.0(−21)	0.0

[a] Solar fluxes at 1 AU integrated over the corresponding wavelength interval; Strobel (1973) and Hinteregger (1976) for 850–1150, Rottman (1981) for 1200–1850, and Mount et al. (1980) for 1900–2000.
[b] Values denote the initial wavelengths of 50 Å intervals except for 1200 and Ly-α at 1216 with respective intervals of 1200–1210 plus 1220–1250 and 1210–1220.
[c] With units ph cm^{-2} s^{-1} $\Delta\lambda^{-1}$.
[d] Atreya (1986) and Strobel (1969).
[e] Strobel (1969, 1973).
[f] Hamai and Hirayama (1979).
[g] Mount and Moos (1978).

Table 6
Hydrocarbon photodissociation reactions[a]

No.	Reaction		$\phi_{\text{Lyman-}\alpha}$[b]	$\phi_{\text{other }\lambda}$[b]	Reference
(R1)	$H_2 + h\nu$	$\rightarrow 2H$	0.00	1.00	c,d
(R2)	$CH_4 + h\nu$	$\rightarrow {}^3CH_2 + 2H$	0.05	0.00	e
(R3)		$\rightarrow {}^1CH_2 + H_2$	0.41	0.90	e
(R4)		$\rightarrow CH + H + H_2$	0.05	0.00	e
(R5)	$C_2H_2 + h\nu$	$\rightarrow C_2H + H$	$\lambda < 1500$ Å, 0.30	$\lambda > 1500$ Å, 0.06	f
(R6)		$\rightarrow C_2 + H_2$	0.10	0.10	
(R7)	$C_2H_4 + h\nu$	$\rightarrow C_2H_2 + H_2$	0.51	0.51	
(R8)		$\rightarrow C_2H_2 + 2H$	0.49	0.49	
(R9)	$C_2H_6 + h\nu$	$\rightarrow C_2H_4 + H_2$	0.13	0.56	
(R10)		$\rightarrow C_2H_4 + 2H$	0.30	0.14	
(R11)		$\rightarrow C_2H_2 + 2H_2$	0.25	0.27	
(R12)		$\rightarrow CH_4 + {}^1CH_2$	0.25	0.02	
(R13)		$\rightarrow 2CH_3$	0.08	0.01	

[a] Reactions and quantum yields are from Yung et al. (1984) unless otherwise specified.
[b] Quantum yield.
[c] Mentall and Gentieu (1970).
[d] Gladstone (1982).
[e] Gladstone et al. (1996).
[f] Okabe (1983).

we have seen in this work is that a synergistic relationship exists between the modeling and the measurements which may reveal surprises, viz., HD vibrational chemistry impacts D in the thermosphere, CH_3D and C_2H_5D are vibrationally enhanced in the thermosphere, and variations in abundance of CH_3D and C_2H_5D in the thermosphere may reflect dynamical activity (i.e., K_h) in the jovian upper atmosphere. These are examples of testable phenomena and an observing program dedicated providing such measurements would provide further insight to the aeronomy of the jovian atmosphere.

Acknowledgments

C.D. Parkinson thanks G.R. Gladstone of SWRI for the use of his radiative transfer code. L. Ben Jaffel and C.D. Parkinson thank CNRS and INSU for continuing support through the PNP Program. C.D. Parkinson acknowledges that some of this work was supported by the National Aeronautics and Space Administration through the NASA Astrobiology Institute under Cooperative Agreement No. CAN-00-OSS-01 and issued through the Office of Space Science. J. McConnell thanks the Natural Sciences and Engineering Research Council of Canada for continuing support. Part of this work was done at York University. Y.L. Yung and A.Y.-T. Lee acknowledge support by NASA Grant NASA5-13296 to the California Institute of Technology.

Appendix A. Chemical model

The solar fluxes and absorption cross-sections used in the calculations are listed in Table 5. The wavelength interval of integration is from 1000 to 2000 Å divided into 50 Å bins with the exception of a separate bin at 1215.67 Å. Wavelengths below 1000 Å are not included since the corresponding solar radiation is significantly absorbed by molecular hydrogen in the upper atmosphere. Tables 6–8 to give the photodissociation reactions, two-body reactions and three-body reactions, respectively.

We have only employed chemistry up to and including C_2H_x species for these simulations. We have used the rate constant data assembled by Romani et al. (1993) and modified by Romani (1996). Parkinson et al. (1999) found it difficult to reconcile their calculated C_2H_2 to C_2H_6 ratio in the μbar pressure region from their simulations with those presented by Gladstone et al. (1996) using the Caltech/Jet Propulsion Laboratory KINETICS model. A similar problem has been noted by Romani (1996). This discrepancy is clearly illustrated by comparing sample model runs plotted in Figs. 11 and 12. A recent intercomparison between the reaction set of Gladstone et al. (1996) and those presented in this work has reconciled this difference. Detailed testing showed that differences in five key reactions caused this discrepancy and they are listed in Table 9. Updating these reactions in KINETICS to correspond with those used in this paper are plotted in Fig. 13 and a com-

Table 7
Hydrocarbon two-body reactions[a]

No.	Reaction		Rate constant, k[b]	Reference
(R14)	$H + {}^1CH_2$	$\rightarrow CH + H_2$	2.0×10^{-10}	c
(R15)	$H + C_2H_3$	$\rightarrow C_2H_2 + H_2$	5.0×10^{-11}	d
(R16)	$H + C_2H_5$	$\rightarrow C_2H_4 + H_2$	3.0×10^{-12}	e
(R17)	${}^1CH_2 + H_2$	$\rightarrow {}^3CH_2 + H_2$	1.26×10^{-11}	
(R18)		$\rightarrow CH_3 + H$	9.24×10^{-11}	
(R19)	${}^1CH_2 + CH_4$	$\rightarrow {}^3CH_2 + CH_4$	1.20×10^{-11}	
(R20)		$\rightarrow 2CH_3$	6.0×10^{-11}	
(R21)	${}^3CH_2 + {}^3CH_2$	$\rightarrow C_2H_2 + C_2H_2$	3.0×10^{-10}	
(R22)	${}^3CH_2 + CH_3$	$\rightarrow H + C_2H_4$	7.0×10^{-11}	f
(R23)	${}^3CH_2 + C_2H_3$	$\rightarrow CH_3 + C_2H_2$	8.0×10^{-11}	c
(R24)	${}^3CH_2 + C_2H_5$	$\rightarrow CH_3 + C_2H_4$	3.0×10^{-11}	
(R25)	$C_2H + C_2H_2$	$\rightarrow C_4H_2 + H$	1.5×10^{-10}	

[a] Reactions and rates are from Yung et al. (1984) unless otherwise specified.
[b] $cm^3\ s^{-1}$.
[c] Moses et al. (2000).
[d] Gladstone et al. (1996).
[e] Tsang and Hampson (1986).
[f] Baulch et al. (1992).

Table 8
Hydrocarbon three-body reactions[a]

No.	Reaction	Rate constants[b]	Reference
(R26)	$H + H \rightarrow H_2$	$1.5 \times 10^{-29} T^{-1.30}$	c
(R27)	$H + {}^3CH_2 \rightarrow CH + H_2$	$4.70 \times 10^{-10} e^{-370/T}$	
(R28)	$H + {}^3CH_2 \rightarrow CH_3$	$3.10 \times 10^{-30} e^{457/T}$	d
		1.50×10^{-10}	
(R29)	$H + CH_3 \rightarrow CH_4$	$3.8 \times 10^{-28} e^{-20/T}$ $T < 200°$	e
		$5.8 \times 10^{-29} e^{-355/T}$ $T > 200°$	
		$1.0 \times 10^{-9} T^{-0.4}$	
(R30)	$H + CH_4 \rightarrow CH_3 + H_2$	$3.37 \times 10^{-20} T^3 e^{-4406/T}$	e
(R31)	$H + C_2H_2 \rightarrow C_2H_3$	2.60×10^{-31}	d
		$3.8 \times 10^{-11} e^{-1374/T}$	
(R32)	$H + C_2H_3 \rightarrow C_2H_2 + H_2$	1.49×10^{-27}	f
		1.55×10^{-10}	
(R33)	$H + C_2H_4 \rightarrow C_2H_5$	$2.15 \times 10^{-29} e^{-349/T}$	d
		$4.95 \times 10^{-11} e^{-1051/T}$	
(R34)	$H + C_2H_5 \rightarrow 2CH_3$	$7.95 \times 10^{-11} e^{-127/T}$	
(R35)	$H + C_2H_5 \rightarrow C_2H_6$	$5.50 \times 10^{-23} T^{-2} e^{-1040/T}$	d
(R36)	$CH + H_2 \rightarrow {}^1CH_2 + H$	$2.38 \times 10^{-11} e^{-1760/T}$	
(R37)	$CH + H_2 \rightarrow CH_3$	$8.75 \times 10^{-31} e^{524/T}$	d
		8.30×10^{-11}	
(R38)	$CH + CH_4 \rightarrow C_2H_4 + H$	$2.5 \times 10^{-11} e^{-200/T}$	
(R39)	$CH + C_2H_2 \rightarrow C_2H_4 + H$	$1.75 \times 10^{-10} e^{61/T}$	
(R40)	$CH + C_2H_4 \rightarrow C_2H_4 + H$	$2.23 \times 10^{-10} e^{173/T}$	
(R41)	$CH_3 + CH_3 \rightarrow C_2H_6$	$8.76 \times 10^{-7} T^{-7.03} e^{-1390/T}$ $T > 296°$	d
		$1.50 \times 10^{-7} T^{-1.18} e^{-329/T}$	
and		$1.80 \times 10^{-16} T^{-3.75} e^{-300/T}$ $T < 296°$	
		6.0×10^{-11}	
(R42)	$CH_3 + C_2H_3 \rightarrow CH_4 + C_2H_2$	3.40×10^{-11}	
(R43)	$CH_3 + C_2H_5 \rightarrow CH_4 + C_2H_4$	$3.25 \times 10^{-11} T^{-0.5}$	
(R44)	$C_2 + H_2 \rightarrow C_2H + H$	$1.77 \times 10^{-10} e^{-1469/T}$	
(R45)	$C_2 + CH_4 \rightarrow C_2H + CH_3$	$5.05 \times 10^{-11} e^{-297/T}$	g
(R46)	$C_2H + H_2 \rightarrow C_2H_2 + H$	$5.6 \times 10^{-11} e^{-1443/T}$	
(R47)	$C_2H + CH_4 \rightarrow C_2H_2 + CH_3$	$6.94 \times 10^{-12} e^{-250/T}$	
(R48)	$C_2\,H + C_2H_6 \rightarrow C_2H_2 + C_2H_5$	$3.5 \times 10^{-11} e^{3/T}$	h
(R49)	$C_2H_3 + H_2 \rightarrow C_2H_4 + H$	$5.0 \times 10^{-20} T^{2.63} e^{-4298/T}$	f
(R50)	$C_2H_3 + CH_3 \rightarrow C_2H_2 + CH_4$	6.5×10^{-13}	
(R51)	$2C_2H_3 \rightarrow C_2H_4 + C_2H_2$	2.40×10^{-11}	
(R52)	$C_2H_3 + C_2H_5 \rightarrow C_2H_2 + C_2H_6$	2.81×10^{-12}	
(R53)	$\rightarrow C_2H_4 + C_2H_4$	2.81×10^{-12}	
(R54)	$2C_2H_5 \rightarrow C_2H_6 + C_2H_4$	2.30×10^{-11}	i

[a] Reactions and rates are from Yung et al. (1984) unless otherwise specified.
[b] Most of the three-body rate coefficients, in $cm^6\ s^{-1}$, are set as $k = k_0 k_\infty / (k_0 M + k_\infty)$. k_0 is listed first above k_∞.
[c] Trauger et al. (1973).
[d] Romani et al. (1993).
[e] Gladstone et al. (1996).
[f] Romani (1996).
[g] Pitts et al. (1982).
[h] Opansky (1996).
[i] Berman et al. (1982).

parison of this figure with Fig. 12 shows close agreement now between the models.

Although the studies of both Gladstone et al. (1996) and Romani (1996) included hydrocarbon chemistry up to C_4 species, this should not have a large impact our results. In the μbar pressure region an important difference in the two compilations is in the pressure dependence of the $CH_3 + H \rightarrow CH_4$ and $CH_3 + CH_3 \rightarrow C_2H_6$ recombination reactions. We employ the reaction of Romani et al. (1993) for the former and a modified version (Lee et al., 2000) of the reaction originally given by Slagle et al. (1988) for the latter.

Table 9
Reaction comparison between KINETICS and this work

No.	Reaction	Comments
1	$H + CH_3 + M \rightarrow CH + H_2 + M$	Both models
2	$H + CH \rightarrow C + H_2$	In KINETICS only
3	$H + C_2H_4 + M \rightarrow C_2H_5 + M$	Both models
4	$C + H_2 + M \rightarrow {}^3CH_2 + H$	In KINETICS only
5	$C_2H + H_2 \rightarrow C_2H_2 + H$	Both models

Romani (1996) has updated his reaction scheme using recent measurements of rate constants and products for the reactions:

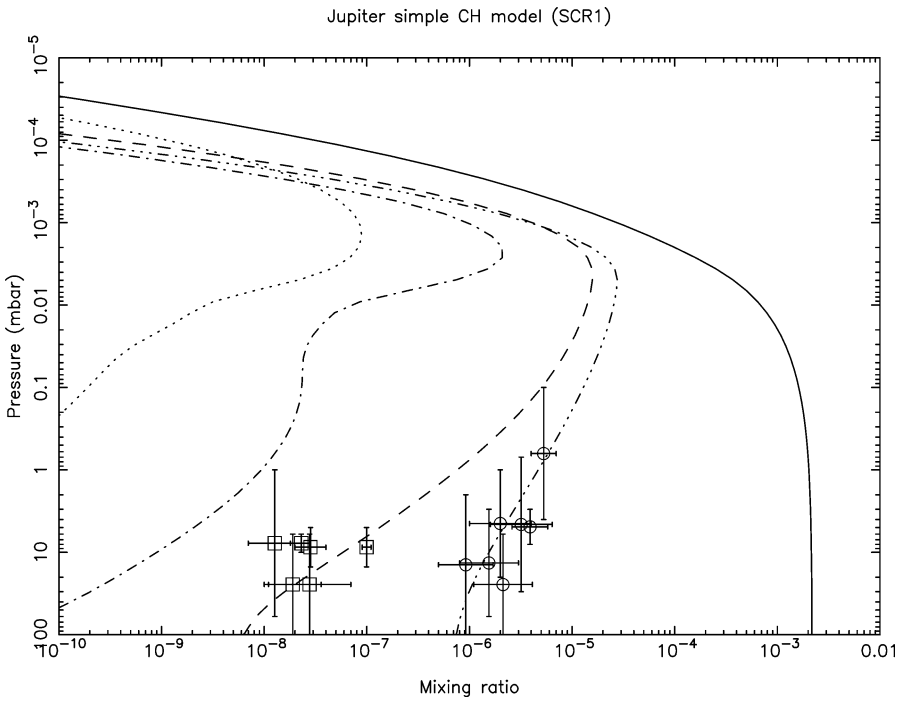

Fig. 11. Model mixing ratios for hydrocarbons on Jupiter (Lee and Yung, 2001): CH_4 (solid), C_2H_2 (dashed), C_2H_4 (dash–dot), C_2H_6 (dash–dot–dot–dot), and CH_3 (dotted). Voyager IRIS and ground based observations: C_2H_2 (open square) and C_2H_6 (open circle).

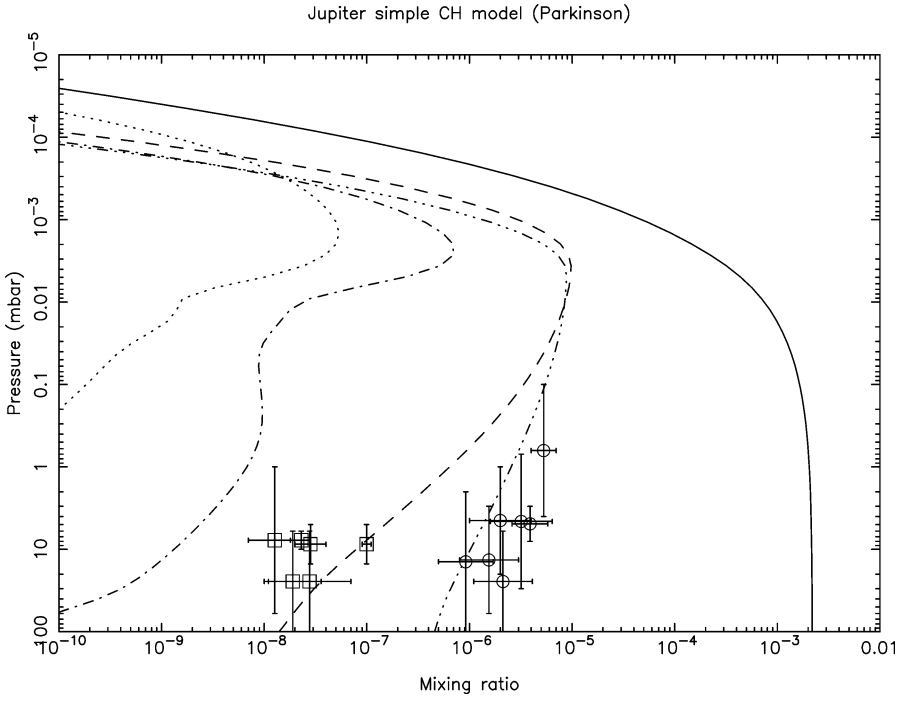

Fig. 12. Model mixing ratios for hydrocarbons on Jupiter (Parkinson, 2002): CH_4 (solid), C_2H_2 (dashed), C_2H_4 (dash–dot), C_2H_6 (dash–dot–dot–dot), and CH_3 (dotted). Voyager IRIS and ground based observations: C_2H_2 (open square) and C_2H_6 (open circle).

$$C_2H_3 + H_2 \rightarrow C_2H_4 + H \quad \text{(A.1)}$$

and

$$C_2H_3 + H \rightarrow H_2 + C_2H_2 \text{ (a)},$$
$$\xrightarrow{M} C_2H_4 \text{ (b)}. \quad \text{(A.2)}$$

The measurements of Fahr et al. (1995) at room temperature combined with an estimate of the temperature dependence from Tsang and Hampson (1986) provide a rate constant for Eq. (A.1) that is much slower than that used earlier by Romani et al. (1993) and Gladstone et al. (1996) and indicates that it will not be of importance under most conditions in the lower stratospheres of the outer planets. In addition, recent measurements by Monks et al. (1995) on reaction (A.2) show that channel (b) is important. Romani (1996) has integrated information

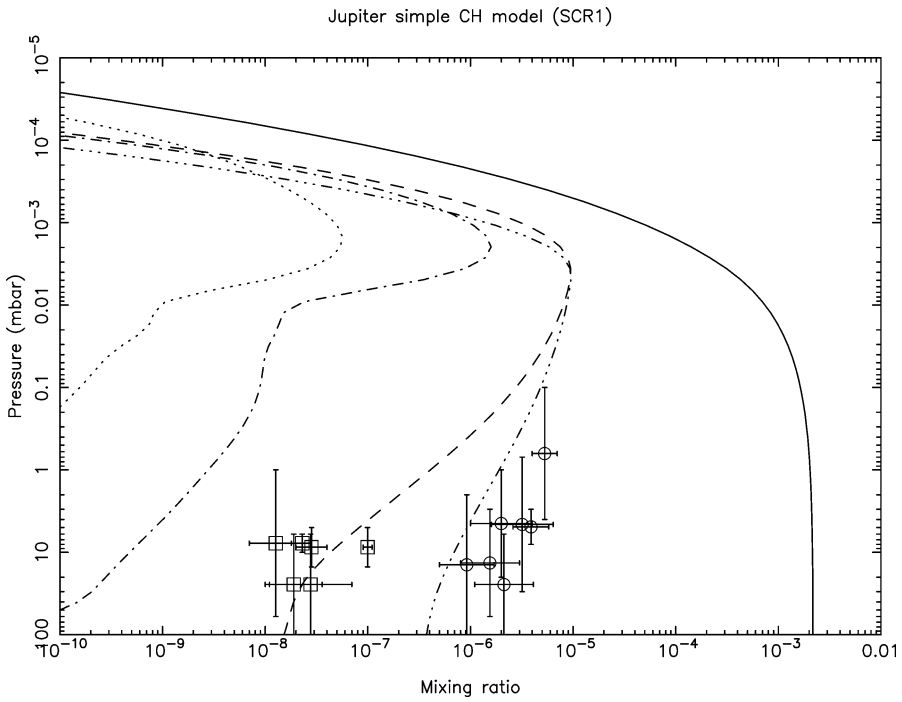

Fig. 13. Model mixing ratios for hydrocarbons on Jupiter (Lee and Yung, 2001) model atmosphere updated to Parkinson (2002): CH_4 (solid), C_2H_2 (dashed), C_2H_4 (dash–dot), C_2H_6 (dash–dot–dot–dot), and CH_3 (dotted). Voyager IRIS and ground based observations: C_2H_2 (open square) and C_2H_6 (open circle).

on the rate from Monks et al. (1995) and Fahr et al. (1995) to estimate the rate constants for the abstraction and recombination channels for reaction (A.2).

Equation (13) is solved using a finite central difference approximation for the vertical derivatives and the species densities are solved semi-implicitly using a simple tridiagonal solver. For these applications we have assumed a steady state exists and so have driven the solution so that $\partial n_i/\partial t \to 0$.

References

Abgrall, H., Roueff, E., Launay, F., Roncin, J.Y., Subtil, J.L., 1993. Table of the Lyman band system of molecular-hydrogen. Astron. Astrophys. Suppl. 101 (2), 273–321.

Aoiz, F., Bañares, J., Dìez-Rojo, T., Herrero, V.J., Sáez Rábanos, V., 1996. Reaction cross section and rate constant calculations for the $D + H_2$ ($v = 0, 1$) $\to$ HD + H reaction on three ab initio potential energy surfaces. A quasiclassical trajectory study. J. Phys. Chem. 100, 4071–4083.

Atreya, S.K., 1986. Atmospheres and Ionospheres of the Outer Planets and Their Satellites. Springer-Verlag, New York.

Atreya, S.K., Edgington, S.G., Encrenaz, Th., Feuchtgruber, H., 1999. ISO observations of C_2H_2 on Uranus and CH_3 on Saturn: Implications for atmospheric vertical mixing in the Voyager and ISO epochs, and a call for relevant laboratory data. In: Cox, P., Kessler, M.F. (Eds.), Universe as Seen by Infrared Space Observatory. ESA SP-427, pp. 149–152.

Baulch, D.L., Cobos, C.J., Cox, R.A., Esser, C., Frank, P., Just, Th., Kerr, J.A., Pilling, M.J., Troe, J., Walker, R.W., Warnatz, J., 1992. Evaluated kinetic data for combustion modeling. J. Phys. Chem. Ref. Data 21, 411–736.

Beer, R., Taylor, F.W., 1973. The abundance of CH_3D and the D/H ratio in Jupiter. Astrophys. J. 179, 309–327.

Beer, R., Taylor, F.W., 1978. The D/H and C/H ratios in Jupiter from the CH_3D phase. Astrophys. J. 219, 763–767.

Ben Jaffel, L., Clarke, J.T., Prangé, R., Gladstone, G.R., Vidal-Madjar, A., 1993. The Lyman alpha bulge of Jupiter: Effects of non-thermal velocity field. Geophys. Res. Lett. 20, 747–750.

Ben Jaffel, L., Vidal-Madjar, A., Gladstone, G.R., McConnell, J.C., Emmerich, C., Prangé, R., Clarke, J.T., 1998. GHRS detection of the fossil deuterium of Jupiter. In: The Scientific Impact of the GHRS. In: ASP Conf. Series, vol. 143, p. 366.

Berman, M.R., Fleming, J.W., Harvey, A.B., Lin, M.C., 1982. Temperature dependence of the reactions of CH radicals with unsaturated hydrocarbons. Chem. Phys. 73, 27–33.

Bézard, B., Encrenaz, Th., Lellouch, E., Feuchtgruber, H., 1999. A new look at the jovian planets. Science 283, 800–801.

Broadfoot, A.L., Sandel, B.R., Shemansky, D.E., McConnell, J.C., Smith, G.R., Holberg, J.B., Atreya, S.K., Donahue, T.M., Strobel, D.F., Bertaux, J.L., 1981. Overview of the Voyager ultraviolet spectrometry results through Jupiter encounter. J. Geophys. Res. 86, 8259–8284.

Broadfoot, A.L., Atreya, S.K., Bertaux, J.L., Blamont, J.E., Dessler, A.J., Linick, S., 1989. Ultraviolet Spectrometer observations of Neptune and Triton. Science 246, 1459–1466.

Buchenau, H., Toennies, J.P., Arnold, J., Wolfrum, J., 1990. $H + H_2$: The current status. Ber. Busenges. Phys. Chem. 94, 1231–1248.

Bush, B.C., Chakrabarti, S., 1995. Analysis of Lyman α and He I 584-Å airglow measurements using a spherical radiative transfer model. J. Geophys. Res. 100, 19609–19625.

Chamberlain, J.W., Hunten, D.M., 1987. Theory of Planetary Atmospheres: An Introduction to Their Physics and Chemistry. Academic Press, Toronto.

Clarke, J.T., Gladstone, G.R., Ben Jaffel, L., 1991. Jupiter's dayglow H Ly α emission line profile. Geophys. Res. Lett. 18, 1935–1938.

Cody, R.J., Romani, P.N., Nesbitt, F.L., Iannone, M.A., Tardy, D.C., Stief, L.J., 2003. Rate constant for the reaction $CH_3 + CH_3 \to C_2H_6$ at $T = 155$ K and model calculation of the CH_3 abundance in the atmospheres of Saturn and Neptune. J. Geophys. Res. 108, 5-1–5-16.

Cravens, T.E., 1987. Vibrationally excited molecular hydrogen in the upper atmosphere of Jupiter. J. Geophys. Res. 92, 11083–11100.

Dreier, T., Wolfrum, J., 1986. Experimental study of the $D + H_2$ ($v = 1$) reaction by CARS spectroscopy. Int. J. Chem. Kinet. 18, 910–935.

Emerich, C., Ben Jaffel, L., Clarke, J.T., Prangé, R., Gladstone, G.R., Sommeria, J., Ballester, G., 1996. Evidence for supersonic turbulence in the upper atmosphere of Jupiter. Science 273, 1085–1087.

Encrenaz, Th., de Graauw, T., Schaeidt, S., Lellouch, E., Feuchtgruber, H., Beintema, D.A., Bézard, B., Drossart, P., Griffin, M., Heras, A., Kessler,

M., Leech, K., Morris, P., Roelfsema, P.R., Roos-Serote, M., Salama, A., Vandenbussche, B., Valentijn, E.A., Davis, G.R., Naylor, D.A., 1996. First results of ISO–SWS observations of Jupiter. Astron. Astrophys. 315, L397–L400.

Fahr, A., Monks, P.S., Stief, L.J., Laufer, A.H., 1995. Experimental determination of the rate constant for the reaction of C_2H_3 with H_2 and implications for the partitioning of hydrocarbons in atmospheres of the outer planets. Icarus 116, 415–422.

Festou, M.C., Atreya, S.K., Donahue, T.M., 1981. Composition and thermal profiles of the jovian upper atmosphere determined by the Voyager Ultraviolet Stellar Occultation experiment. J. Geophys. Res. 86, 5715–5725.

Gladstone, G.R., 1982. Radiative Transfer and Photochemistry in the Upper Atmosphere of Jupiter. Ph.D. thesis, California Institute of Technology, Pasadena.

Gladstone, G.R., 1988. UV resonance line dayglow emissions on Earth and Jupiter. J. Geophys. Res. 93, 14623–14630.

Gladstone, G.R., Allen, M., Yung, Y.L., 1996. Hydrocarbon photochemistry in the upper atmosphere of Jupiter. Icarus 119, 1–52.

Griffioen, E., 2000. A pseudo-three-dimensional resonance line radiative transfer model with overlapping lines. J. Geophys. Res. Space Phys. 105, 24613–24620.

Griffioen, E., McConnell, J.C., Shepherd, G.G., 1994. Rapidly convergent lambda operator method for solving resonance line scattering in planetary atmospheres. 1. The one-dimensional slab. J. Geophys. Res. 99, 21383–21396.

Hamai, S., Hirayama, F., 1979. Fluorescence of acetylenic hydrocarbons. J. Chem. Phys. 71, 2934–2939.

Hinteregger, H.E., 1976. EUV fluxes in the solar spectrum below 2000 Å. J. Atmos. Terr. Phys. 38, 791–806.

Lean, J., 1987. Solar ultraviolet irradiance variations: A review. J. Geophys. Res. 92, 839–868.

Lean, J., 1991. Variations in the Sun's radiative output. Rev. Geophys. 29, 505–535.

Lee, A.Y.T., Yung, Y., 2001. Photochemical modeling of CH_3 abundances in the outer Solar System. J. Geophys. Res. 105, 20207–20225.

Lee, A.Y.T., Yung, Y., Cheng, B., Bahou, M., Chung, C., Lee, Y., 2000. Enhancement of deuterated ethane on Jupiter. Astrophys. J. 551, L93–L96.

Lellouch, E., Encrenaz, Th., de Graauw, Th., Schaeidt, S., Feuchtgruber, H., Beintema, D.A., Bézard, B., Drossart, P., Griffin, M., Heras, A., Kessler, M., Leech, K., Morris, A., Roelfsema, P.R., Roos-Serote, M., Salama, A., Vandenbussche, B., Valentijn, E.A., Davies, G.R., Naylor, D.A., 1996. Delimination of the D/H ratio on Jupiter from ISO/SWS observations. Bull. Am. Astron. Soc. 28, 1148. 22.34.

Lemaire, P., Charra, J., Jouchoux, A., Vidal-Madjar, A., Artzner, G.E., Vial, J.C., Bonnet, R.M., Skumanich, A., 1978. Calibrated full disk H I Lyman-α and Lyman-β profiles. Astrophys. J. 223, L55–L58.

Mahaffy, P.R., Donahue, T.M., Atreya, S.K., Owen, T.C., Niemann, H.B., 1998. Galileo Probe measurements of D/H and ^{3}He/^{4}He in Jupiter's atmosphere. Space Sci. Rev. 84, 251–263.

Majeed, T., McConnell, J.C., Yelle, R.V., 1991. Vibrationally excited H_2 in the outer planets: Role of the fluorescence source. Planet. Space Sci. 39, 1591–1606.

Mason, E.A., Marrero, T.R., 1970. The diffusion of atoms and molecules. In: Bates, D.R., Esterman, I. (Eds.), Advances in Atomic and Molecular Physics, vol. 6. Academic Press, New York, pp. 155–232.

McConnell, J.C., Holberg, J.B., Smith, G.R., Sandel, B.R., Shemansky, D.E., Broadfoot, A.L., 1982. A new look at the ionosphere of Jupiter in light of the UVS occultation results. Planet. Space Sci. 30, 151–167.

McGrath, M.A., 1991. An unusual change in the jovian Lyman-alpha bulge. Geophys. Res. Lett. 18 (11), 1931–1934.

Meier, R.R., Prinz, D.K., 1970. Absorption of the solar Lyman-α line by geocoronal atomic hydrogen. J. Geophys. Res. 75, 6969–6979.

Mentall, J.E., Gentieu, E.P., 1970. Lyman-α fluorescence from the photodissociation of H_2. J. Chem. Phys. 52, 5641–5645.

Michael, J.V., Fisher, J.R., 1990. Rate constants for the reaction $D + H_2 \rightarrow HD + H$ over the temperature range 655–1979 K, by the flash photolysis-shock tube technique. J. Phys. Chem. 94, 3318–3323.

Mielke, S.L., Lynch, G.C., Truhlar, D.G., Schwenke, D.W., 1994. Ab initio chemical kinetics: Converged quantal reaction rate constants for the $D + H_2$ system. J. Phys. Chem. 98, 8000–8008.

Monks, P.S., Nesbitt, F.L., Payne, W.A., Scanlon, M., Stief, L.F., 1995. Kinetics and products of the reactions between H and C_2H_2 at $T = 213$ K and $T = 398$ K. J. Phys. Chem. 99, 17151–17159.

Moses, J., Bézard, I., Lellouch, E., Gladstone, G.R., Feuchtgruber, H., Allen, M., 2000. Photochemistry of the upper atmosphere of Saturn. I. Hydrocarbon chemistry and comparisons with ISO observations. Icarus 13, 244–298.

Mount, G.H., Moos, H.W., 1978. Photoabsorption cross sections of methane and ethane, 1380–1600 Å at $T = 295$ K and $T = 200$ K. Astrophys. J. 224, L35–L38.

Mount, G.H., Rottman, G.J., Timothy, J.G., 1980. The solar spectral irradiance 1200–2550 Å at solar maximum. J. Geophys. Res. 85, 4271–4274.

Niemann, H.B., Atreya, S.K., Carignan, G.R., Donahue, T.M., Haberman, J.A., Harpold, D.N., Hartle, R.E., Hunten, D.M., Kasprzak, W.T., Mahaffy, P.R., Owen, T.C., Spencer, N.W., Way, S.H., 1996. The Galileo Probe Mass Spectrometer: Composition of Jupiter's atmosphere. Science 272, 849–851.

Okabe, H., 1983. Photochemistry of acetylene. Can. J. Chem. 61, 850–855.

Opansky, B.J., 1996. Low Temperature Rate Coefficients of the Ethynyl Radical. Ph.D. thesis, University of Colorado at Boulder, Boulder, CO.

Parkinson, C.D., 2002. Photochemistry and Radiative Transfer Studies in the Atmosphere of Jupiter and Saturn. Ph.D. thesis, Department of Earth and Space Science, York University, Toronto, Canada.

Parkinson, C.D., Griffioen, E., McConnell, J.C., Gladstone, G.R., Sandel, B.R., 1998. He 584 Å dayglow at Saturn: A reassessment. Icarus 133, 210–220.

Parkinson, C.D., Griffioen, E., McConnell, J.C., Ben Jaffel, L., Vidal-Madjar, A., Clarke, J.T., Gladstone, G.R., 1999. Estimates of atomic deuterium abundance and Lyman-alpha airglow in the thermosphere of Jupiter. Geophys. Res. Lett. 26, 3177–3180.

Pitts, W.M., Pasternack, L., McDonald, J.R., 1982. Temperature dependence of the C_2 ($X^1\Sigma_g^+$) reaction with H_2 and C_2 ($X^1\Sigma_g^+$ and $a^3\Pi_4$ equilibrated states) with O_2. Chem. Phys. 68, 417–422.

Polanyi, J.C., Schreiber, J.L., 1974. The dynamics of bimolecular reactions. In: Jost, W. (Ed.), Physical Chemistry: An Advanced Treatise, vol. 6A. Academic Press, New York, pp. 383–487.

Richards, P.G., Fennelly, J.A., Torr, D.G., 1994. EUVAC: A solar EUV flux model for aeronomic calculations. J. Geophys. Res. 99, 8981–8992. (Correction, 1994. J. Geophys. Res. 99, 13283.)

Romani, P.N., 1996. Recent rate constant and product measurements of the reactions $C_2H_3 + H_2$ and $C_2H_3 + H$—Importance for photochemical modeling of hydrocarbons on Jupiter. Icarus 122, 233–241.

Romani, P.N., Bishop, J., Bézard, B., Atreya, S., 1993. Methane photochemistry on Neptune: Ethane and acetylene mixing ratios and haze production. Icarus 106, 442–463.

Rottman, G.J., 1981. Rocket measurements of the solar spectral irradiance during solar minimum, 1972–1977. J. Geophys. Res. 86, 6697–6705.

Sandel, B.R., Broadfoot, A.L., Strobel, D.F., 1980. Discovery of a longitudinal asymmetry in the H Lyman-alpha brightness of Jupiter. Geophys. Res. Lett. 7, 5–8.

Seakins, P.W., Robertson, S.H., Pilling, M.J., Wardlaw, D.M., Nesbitt, F.L., Thorn, R.P., Payne, W.A., Stief, L.J., 1997. Temperature and isotope dependence of the reaction of methyl radicals with deuterium atoms. J. Phys. Chem. 101, 9974–9987.

Seiff, A., Kirk, D.B., Knight, T.C.D., Mihalov, J.D., Blanchard, R.C., Young, R.E., Schubert, G., von Zahn, U., Lehmacher, G., Milos, F.S., Wang, J., 1997. Thermal structure of Jupiter's upper atmosphere derived from the Galileo Probe. Science 276, 102–104.

Shemansky, D., Tew Hallett, J., Liu, X., Gangopadhyay, P., and the Cassini UVIS Team, 2003. Atmospheric hydrogen physical chemistry: The Jupiter and Uranus dayglows. Bull. Am. Astron. Soc. 35, 1020. 50.12.

Slagle, I.R., Gutman, D., Davies, J.W., Pilling, M.J., 1988. Study of the recombination reaction $CH_3 + CH_3 \rightarrow C_2H_6$. 1. Experiment. J. Phys. Chem. 92, 2455–2462.

Sommeria, J., Ben Jaffel, L., Prangé, R., 1995. On the existence of supersonic jets in the upper atmosphere of Jupiter. Icarus 119, 2–24.

Strobel, D.F., 1969. The photochemistry of methane in the jovian atmosphere. J. Atmos. Sci. 26, 906–911.

Strobel, D.F., 1973. The photochemistry of hydrocarbons in the jovian atmosphere. J. Atmos. Sci. 30, 489–498.

Tobiska, W.K., 1991. Revised solar extreme ultraviolet flux model. J. Atmos. Terr. Phys. 53, 1005–1018.

Tobiska, W.K., 1994. Modeled soft X-ray solar irradiances. Solar Phys. 152, 207–215.

Trauger, J.T., Roesler, F.L., Carleton, N.P., Traub, W.A., 1973. Observation of HD on Jupiter and the D/H ratio. Astrophys. J. 184, L137–L141.

Tsang, W., Hampson, R.F., 1986. Chemical kinetic data base for combustion chemistry. Part 1. Methane and related compounds. J. Phys. Chem. Ref. Data 15, 1087–1279.

Vervack, R.J., Sandel, B.R., Gladstone, G.R., McConnell, J.C., Parkinson, C.D., 1995. Jupiter's He 584 Å dayglow: New results. Icarus 114, 163–173.

Vidal-Madjar, A., 1975. Evolution of the solar Lyman alpha flux during four consecutive years. Solar Phys. 40, 69–86.

von Zahn, U., Hunten, D.M., 1996. The helium mass fraction in Jupiter's atmosphere. Science 272, 849–851.

Waite Jr., J.H., Cravens, T.E., Kozyra, J., Nagy, A.F., Atreya, S.K., Chen, R.H., 1983. Electron precipitation and related aeronomy of the jovian thermosphere and ionosphere. J. Geophys. Res. 88, 6143–6162.

Wong, A.S., Yung, Y.L., Friedson, A.J., 2003. Benzene and haze formation in the polar atmosphere of Jupiter. Geophys. Res. Lett. 30, 1447.

Yelle, R.V., Young, L.A., Vervack Jr., R.J., Young, R., Pfister, L., Sandel, B.R., 1996. Structure of Jupiter's upper atmosphere: Predictions for Galileo. J. Geophys. Res. 101, 2149–2161.

Yung, Y.L., DeMore, W.B., 1999. Photochemistry of Planetary Atmospheres. Oxford Univ. Press, Oxford, UK.

Yung, Y.L., Strobel, D.F., 1980. Hydrocarbon photochemistry and Lyman-α albedo of Jupiter. Astrophys. J. 239, 395–402.

Yung, Y.L., Allen, M., Pinto, J.P., 1984. Photochemistry of the atmosphere of Titan: Comparison between model and observations. Astrophys. J. Suppl. Ser. 55, 465–506.

Yung, Y.L., Friedl, R., Pinto, J.P., Bates, K.L., Wen, J., 1988. Kinetic isotopic fractionation and origin of HDO and CH_3D in the Solar System. Icarus 74, 121–132.